CRYSTALLOGRAPHY OF LOW ALLOY IRON MARTENSITES

by

PAUL WILLIAM JEFFREY

A THESIS SUBMITTED IN PARTIAL FULFILLMENT

OF THE REQUIREMENTS FOR THE DEGREE OF

MASTER OF SCIENCE

IN THE DEPARTMENT

OF

METALLURGY

We accept this thesis as conforming to the

standard required from candidates for

the degree of MASTER OF SCIENCE

Members of the Department of Metallurgy

THE UNIVERSITY OF BRITISH COLUMBIA

April, 1967.

In presenting this thesis in partial fulfilment of the requirements for an advanced degree at the University of British Columbia, I agree that the Library shall make it freely available for reference and study. I further agree that permission for extensive copying of this thesis for scholarly purposes may be granted by the Head of my Department or by his representatives. It is understood that copying or publication of this thesis for financial gain shall not be allowed without my written permission.

Department of **Metallurgy**

The University of British Columbia
Vancouver 8, Canada

Date **May 5, 1967**

ABSTRACT

The morphology and crystallography of the martensite transformation in pure iron and low alloy Fe-C, Fe-Mn, Fe-Mn-Si, Fe-Ni steels which contain no retained austenite was studied. Single surface trace analyses by transmission electron microscopy on directions parallel and normal to the martensite substructure were found to be consistent with the martensite crystals having the form of plates rather than needles. The directions normal to the martensite substructure plates were consistent with a $\{145\}_M$ habit plane.

Optical studies of the martensite surface shears within prior austenite grains revealed that 4 shear variants generally occur. However grains containing 5 or more shear variants could be found which appears to suggest an austenite habit plane close to but different from $\{111\}_A$. A single surface trace analysis of the martensite surface shears using the austenite annealing twin vestiges to orient the grain was consistent with an austenite habit plant $\sim 7^\circ$ from $\{111\}_A$.

Two inhomogeneous shear systems were found to predict the experimental results when applied to the Wechsler, Lieberman, Read theory of martensite transformations. They are $(100)_A[010]_A$ and $(111)_A[\bar{1}\bar{1}2]_A$. The $(111)_A[\bar{1}\bar{1}2]_A$ system is to be generally preferred as its predicted habit planes (7.12° from $\{111\}_A$ and 5.03° from $\{145\}_M$) are more consistent with the trace analyses.

Preliminary work included an investigation of the maraging properties of the Fe-Mn-Si system.

ACKNOWLEDGEMENT

The author would like to extend his sincere thanks to his research director, Dr. D. Tromans for his guidance and help during this work.

The freely given advice and assistance by members of the faculty, staff and student body was invaluable to the completion of this work and is greatly appreciated.

The financial support provided by the National Research Council and Defence Research Board is gratefully acknowledged.

TABLE OF CONTENTS

TABLE OF CONTENTS (continued)

LIST OF FIGURES

LIST OF FIGURES (continued)

LIST OF FIGURES (continued)

LIST OF TABLES

LIST OF TABLES (continued)

INTRODUCTION AND AIM OF INVESTIGATION

This work began as an examination of the transformation substructure and aging characteristics of the martensitic Fe-Mn-Si alloys. The similarity between the Fe-Mn and Fe-Ni binary phase diagrams suggested that a Fe-Mn base maraging steel could be developed in analogy to the commercial Fe-Ni maraging steels. While suggestions of a martensite aging reaction were found the work was largely fruitless; and so it was decided to terminate the aging studies and concentrate on the crystallography and morphology of low alloy ferrous martensites in general. The decision to concentrate on the crystallography and morphology was strengthened by the fact that preliminary studies on the substructure showed deviations from what was generally accepted in the literature. The habit planes in a number of these low alloy martensites were determined. The phenomenological theory of iron martensites as given by Wechsler, Lieberman, and Read was used in an attempt to theoretically explain the experimental results.

The body of the thesis considers the work on the crystallography and morphology while Appendix II contains the preliminary studies carried out on the aging characteristics.

GENERAL FEATURES OF MARTENSITE TRANSFORMATIONS

Some alloys exhibit dual behaviour in that they can transform into different structures depending on the cooling rate. For example, in low nickel steel with an air cool there appears a structure formed by a nucleation and growth process known as equiaxed alpha. But at much higher cooling rates the above nucleation and growth may be too slow and the large driving force (free energy) may become sufficient to cause a shear type of transformation. This is called a martensitic transformation and involves the cooperative movement of many atoms. Evidence that martensitic transformations do not involve atomic interchange lie in the facts that the product phase is of the same composition as the parent, and that alloys already ordered remain ordered after the transformation. A special kind of martensitic transformation is mechanical twinning where the driving force is deformation rather than internal free energy.

The experimental observation most commonly associated with martensitic transformations is the tilting on the surface of a sample which was polished before quenching to martensite. This observed tilting preserves lines (vectors) as lines and planes as planes; for example, a scratch made on a surface before transformation will show no observable discontinuity where it crosses the boundary from parent to product phases. Hence it appears that the product in a martensite transformation is coherent with the parent.

The interface, or plane of contact, between the parent and product phases is called the "Habit Plane"; it is the plane of the lattice along which the martensite plates form. Another experimental feature used to identify a specific transformation is the "Orientation Relationship" which states the parallel planes and parallel directions in the parent and product phases. Rational habit planes or rational pairs of parallel lines and planes are not predicted by current martensite theories.

There are two common types of martensite formed, massive and acicular. Acicular martensite is found in Fe-Ni (30 - 33% Ni) and Fe-C (% C $>$ 0.6) binaries; both acicular martensites are characterized by retained austenite and a twinning shear mode. When the amount of solute (substitutional or interstitial) is sufficient so as to suppress the equiaxed α structure but not so much as to form the acicular structure there appears massive martensite. A polished surface after a massive martensite transformation appears as many shear plates with only a few unique orientations enclosed within the thermally etched prior austenite grain boundaries. Under the electron microscope is observed many parallel martensite plates whose thickness is of the same order as the shear plates; but the relation between the two is not fully understood. Within the martensite plates large tangles of dislocations are seen, hence the reason for considering the dislocation shear mode to be operative. The boundary between the martensite plates is irregular and wavy and could be due to small distortions in the habit plane. It should be noted that the shear plates which form on the polished surface necessarily have different boundary conditions than plates formed within the speciman and hence one must be careful in interpreting their significance.

PREVIOUS WORK

The alloys on which most crystallographic studies have been done are those whose M_s temperature is below room temperature. The reason for this is that in these alloys it is possible to obtain the parent (austenite) and product (martensite) phases coexisting, with the product phase of a size large enough to be observable without optical aid. The habit plane of the martensite crystal can then be accurately obtained by two surface trace analysis. The orientation relationship between the two phases can be found by straddling a martensite plate with an X-ray beam so that the photograph will contain reflections from the austenite as well as from the martensite.

In alloys with low amounts of solute (both interstitial and substitutional) M_f is above room temperature, hence there is no retained austenite. The habit plane can only be determined by the method of single surface trace analysis which is very hard pressed in most cases to give an unique result. The orientation relationship cannot be determined without both phases being present.

The martensitic transformation has been observed in pure iron by Bibby and Parr (1) and Wayman and Altstetter (2). Wayman and Altstetter found the surface shears to be consistent with an apparent $\{111\}_A$ habit plane and the martensite crystals to be plate-like rather than needle-like. It should be noted that needles which lie along $\langle 110\rangle_A$ can appear to have a pseudo $\{111\}_A$ habit plane (3).

One of the definitive papers in the crystallography of Fe-C is that due to Greninger and Troiano (4). They found, through a two surface trace analysis of the twin band vestiges, that in steels with $\%C > 1.4$ the martensite plates were parallel to $\{259\}_A$, with $0.4\% < C < 1.4\%$ the plates were parallel to $\{225\}_A$, while in steels with $C < 0.4\%$ the martensite crystals were needle shaped and formed in a plate-like array along the $\{111\}_A$ planes.

Bowles (5) found that the $\{111\}_A$ habit plane is comprised of laths parallel to a $\langle 101\rangle_A$ direction and is not therefore a true habit plane. Kelly and Nutting (6) by the method of single surface trace analysis found that the long axis of the martensite crystals were parallel to $\langle 111\rangle_M$, while the traces normal to the crystals were not consistent with any particular plane. Hence they concluded that the martensite crystals are likely needles rather than plates. If the Kurdjumov-Sachs orientation relationship is assumed then $\langle 111\rangle_M$ is parallel to $\langle 110\rangle_A$. This $\langle 110\rangle_A$ direction has been reported by other workers (4,5,7).

It is not known for sure whether the crystallography of stainless steels is the same as low carbon alloys, but work such as that done by Kelly and Nutting support the view. They found two different types of martensite, one type as in high carbon steels and a 20% Ni - 0.8% C steel had a plate-like substructure which was internally twinned while the second type as in low carbon and 18 - 8 stainless steels had a substructure composed of so called needles which were not internally twinned.

Owen, Wilson and Bell (8) state that they observed only 4 different massive martensite shear traces within any volume formed from a single austenite grain. This was taken as evidence that the martensite crystals form on the $\{111\}_A$ planes. The appearance of the surface shears in Fe-Mn binaries has been found to be very similar to those in Fe-Ni.

Scatter has been observed (9,10) in crystallographic determinations of the $\{259\}_A$ habit plane, that is greater than that attributable to experimental technique. The scatter is perhaps partially explainable by slight internal stresses which distort the habit plane, but this cannot be the complete answer as the calculated poles due to such a stress lie on a curve in the stereographic triangle, where as observed scatter (10) is as great normal to this curve as along it.

Though quite a number of phenomenological crystallographic theories have been published three of them have gained the widest acceptance; they are those due to Wechsler, Lieberman, Read (WLR) (11, 12), Bowles, MacKenzie (BM) (13) and Bullough, Bilby (BB) (14). The WLR theory assumes that the habit plane is undistorted and unrotated while the BM theory assumes the habit plane to be unrotated but does allow small distortions in the region of one percent. The BB theory assumes an undistorted habit plane but enables other parameters to be readily varied. All three of these theories are essentially equivalent in that they are based on the idea that the total shape deformation accompanying the martensite transformation is, at least approximately, an invariant plane strain. Comparisons of the 3 theories are contained in (15, 16, 17). In the iron base martensites these theories have been able to predict the $\{259\}_A$ and $\{3, 10, 15\}_A$ habit planes but are not so successful with the $\{225\}_A$, unless a 1.5% dilation of the habit plane is allowed. Recently a theory by Lieberman and Bullough (13) which incorporates the observation that martensite plates with a $\{225\}_A$ habit are composite (consist of twinned and untwinned regions) appears to account for the $\{225\}_A$ habits.

With all three of the theories it is possible to predict the austenite and martensite habit planes from a knowledge of the lattice parameters of the austenite and martensite and of the slip system operative. A given slip system is used or disgarded on the following basis: (1) the calculated habit plane corresponds to that determined experimentally (2) the values of g, the lattice invariant shear, and S, the macroscopic shear, must be relatively small, (3) the slip system should be one commonly operative in that type of phase. Wechsler, Read and Lieberman (19) investigated the slip systems along $\{111\}_A$ planes with regard to their applicality to the $\{225\}_A$ habit. Of more interest to the present work though was the fact that the slip system $(111)_A[\bar{1}2\bar{1}]_A$ predicts a habit plane close to $\{111\}_A$ and also has relatively small

values of g and S. Otte (20) investigated a number of different slip systems and compared the calculated habit planes to those commonly observed experimentally; also considered was the effect which variations in the volume ratio of martensite to austenite has on the calculated habit planes. Computer programs were used by Crocker and Bilby (21) with the Bullough and Bilby theory to examine the crystallographic features of martensite reactions in steels. One interesting comment they make is that virtually any habit plane could be predicted by making a suitable choice of dislocation shear; hence they had to limit their analysis to those shear systems commonly observed in either the austenite or martensite.

A surface martensite which formed at 20 - 30° C above the M_s temperature for the bulk material has been reported by Honma (22) in iron alloys of between 20 and 30% Ni. Similar results were obtained by Klostermann and Burgers (23) in a Fe - 30.2% Ni - 0.4% C alloy. The surface martensite was found to form as needles down to a depth of from 5 → 30 μ. This surface martensite has been explained (24) as being caused by a reduction of the strain energy term which is introduced in calculating the critical embroyo size for martensite formation. The question of the presence of a surface martensite was examined within the department on Fe - 4.8% Cu martensite. Down to a depth of approximately .010 inch the martensite was observed to be uniform with no distinct surface martensite layer.

EXPERIMENTAL

MATERIALS:

The iron stock used has the trade name "Ferrovac E" and was obtained from the Crucible Steel Company of America. The impurities in weight percents were as follows:

C .005, Mn .0005, P .003, S .005, Si .006, Ni .02, Cr .006, V .004, W .01, Mo .001, Co .006, N .00085, O_z .0030, H_z .000025, Cu .01.

Ferrosilicon was obtained from Esco Refinery of Port Coquitlam. The silicon content was analyzed to be 86.7 wt.%.

Electrolytic manganese was used in preparing alloys.

ALLOY PREPARATION:

Four of the six alloys studied were prepared by induction melting under an argon atmosphere. A fused magnesia crucible was used but because these invariably crack it was found necessary to place them inside larger silicon carbide crucibles. The gap between the two crucibles was filled with alumina and sealed with refractory cement. The iron was melted first, then the ~~manganese and silicon~~ ALLOYING ADDITIONS added portion by portion, waiting 4 to 5 minutes between each portion to allow thorough melting and stirring of the fresh charge. This procedure is most important as several melts were found to be in inhomogeneous. The heats were chill casts into iron moulds. The quantity of each alloy cast was approximately 300 gms.

The Fe - .17% C alloy used was a commercial mild steel. The pure iron "alloy" was Ferrovac E.

ALLOY ANALYSIS

The compositions of the six alloys studied were analysed to be:

(1) Pure iron
(2) Fe - .06% C
(3) Fe - .17% C

(4) Fe - 6.0% Mn
(5) Fe - 1.7% Si - 7.83% Mn
(6) Fe - 10.79% Ni

The Fe- 6.0% Mn alloy was analysed (along with those listed in the Appendix II) by X-ray fluorescence, while the Fe - 1.7% Si - 7.83% Mn and Fe - 10.79% Ni alloys were analysed chemically. The carbon alloys were analysed by burning a sample of known weight in pure oxygen, collecting and weighing the CO_2 formed, and then calculating the Wt. % C in the sample.

The method used for the analysis by X-ray fluorescence is as follows. Six alloys as listed in Appendix II were chemically analysed, these were used as standards in the determination of the calibration chart which compares the ratio of the heights of the manganese $K\alpha_1$, $K\alpha_2$ peak and iron $K\beta_1$ peak against percent manganese. The fact that there was a 3rd element present, silicon up to 6 percent, will slightly affect the accuracy of the calibration curve.

Specimans used on the X-ray fluorescence unit were approximately $\frac{3}{4}$" x $\frac{3}{4}$" x $\frac{1}{4}$" with one face polished on 3/0 grit paper.

SURFACE SHEARS:

The surface shears caused by the martensitic transformation were studied as follows. Samples approximately $\frac{3}{4}$" x $\frac{3}{4}$" were polished either electrolytically or with diamond paste. Samples of pure iron, Fe - .06% C, and Fe - .17% C were .030 in. thick while those of Fe - 6.0% Mn, Fe - 1.7% Si - 7.83% Mn, and Fe - 10.79% Ni were about 0.100 in. thick. The specimans were suspended in a dissociated ammonia atmosphere ($3H_2 + N_2$) for $1\frac{1}{2}$ hours at a temperature of approximately 1250°C. The presence of nitrogen in the atmosphere appeared to have no effect on the surface shears formed as specimans which were treated in a pure H_2 atmosphere gave similar shear configurations. A soaking time of $1\frac{1}{2}$ hours was used to ensure stabilization of the austenite grain growth. It was found necessary to quench from a temperature as high as 1250°C because otherwise the austenite grains were so small as to inhibit

formation of the martensite surface shears. After soaking at 1250°C the specimans were quenched directly into brine, at which time the surface shears formed on the pre-polished surface.

ELECTRON MICROSCOPY:

Material to be used for electron microscopy was first hot rolled from the cast thickness of 0.5 inch down to approximately .040 inch. The surfaces were cleaned of oxide in a warmed 15% solution of sulfuric acid in water and subsequently cold rolled, to obtain a smooth surface, down to a thickness of .025 inch. Samples of approximately $\frac{3}{4}$ x $\frac{3}{4}$ inch were cut from the sheet, annealed at 1050°C for 1 hour in a $3H_2+N_2$ atmosphere and then quenched into brine. The sample was then chemically polished down to a thickness of about .003 inch in a warmed solution of the following composition:

HCl	20 c.c.
H_3PO_4	20 c.c.
HNO_3	50 c.c.
CH_3COOH	100 c.c.

It was necessary to stir the solution vigorously so as to ensure an even attack. Because the chemical polishing solution rapidly decomposes it must be discarded after polishing each speciman.

Choosing the thinnest areas left by the chemical polishing process the speciman was electropolished by the Bollman technique (25) in a solution of the following composition:

Water	7 c.c.
Chromic Acid	25 gms.
Acetic Acid	135 c.c.

The foils were studied using a Hitachi Hu - 11A electron microscope at an accelerating voltage of 100 KV.

Single Surface Trace Analyses

Single surface trace analyses were used to investigate the austenite and martensite habit planes.

The austenite habit plane was investigated using the austenite annealing twin vestiges to orient the grain with respect to the austenite axes. This can be done by finding 3 twin vestiges within any one prior austenite grain and by using the fact that the twinning plane in the austenite is $\{111\}$. In this analysis it was possible to obtain any number up to 4 traces from one oriented grain. The analysis was carried out by optical microscope at 200X.

Transmission electron microscopy was used to investigate the martensite habit plane. The zone axis of the plane of the image was obtained from a selected area diffraction pattern of the substructure plate under consideration. Each substructure plate was oriented by comparing with specific crystallographic directions on the selected area diffraction pattern.

RESULTS

SURFACE SHEARS

All six of the alloys studied were found to undergo a martensitic transformation as evidenced by the presence of surface shears on a speciman polished before quenching. The surface shears were found to be limited by the boundaries of the austenite grains which were thermally etched during the austenizing treatment. Only a small number of orientations to the surface shears were found within any one prior austenite grain, with 4 being the greatest number commonly observed. But in all six alloys areas were observed where 5, 6 or 7 traces were present (figs. 3, 5, 7, 9, 11, 13). The appearance of the surface shears for all six alloys was very similar.

Tables 1 to 4 give the stated angular measurements made during the single surface trace analysis of the surface shears in the Fe - .17% C and Fe - 6.0% Mn alloys. Fig. 15 shows the typical appearance of the annealing twin vestiges.

ELECTRON MICROSCOPY

A single surface trace analysis was carried out on all six alloys. The great circles connecting the directions parallel and normal to the martensite crystals with the zone of the surface, are plotted in Figs. 16, 18, 20, 22, 24, 26 and 17, 19, 21, 23, 25, 27 respectively. The angles which the above great circles for directions normal to the crystals make with each of $\{100\}_M$, $\{011\}_M$, $\{111\}_M$, $\{112\}_M$, $\{145\}_M$, and the calculated plane* are given in tables 5 to 10. The great circles for directions parallel to the martensite crystals are compared with the directions $\langle 111\rangle_M$ in table 11.

Electron micrographs of the martensite substructure are given in Figs. 4, 6, 8, 10, 12, 14.

* Calculated plane refers to that predicted using the system $(111)_A\ [\bar{1}\bar{1}2]_A$ with $V_I = 1.04$ in the Wechsler, Lieberman, Read, Theory.

CALCULATIONS

For the inhomogeneous shears $(111)_A [\bar{1}\bar{1}2]_A$ and $(100)_A [010]_A$ the values of "g" (dislocation shear) and "S" (Shape deformation) were calculated as per appendix I for values of V_I of 1.00, 1.03, 1.04 and 1.08866. The results are contained in table 12. The parallelism between close packed planes and directions in the austenite and martensite for the above slip systems and values of V_I are given in table 13.

The calculated habit planes in the austenite and martensite are given in table 14; with the same results plotted in Stereographic triangles in Figs. 1 and 2.

GRAINS	DEGREES	GRAINS	DEGREES	GRAINS	DEGREES
1	0.5		0.0		0.0
	2.0	4	0.0	7	0.0
	0.5		0.0		4.0
	3.0		2.0		0.0
2	0.5	5	0.5		2.0
	0.0		2.0	8	2.0
	0.0		0.0		0.0
3	1.0	6	0.0		1.0
	0.0		1.0		

Table 1. Fe - .17%C. Annealing twin vestige analysis. Angles are those between surface shear normals and calculated austenite habit plane.

GRAINS	DEGREES	GRAINS	DEGREES	GRAINS	DEGREES
1	2.0		4.0		2.0
	0.0	4	9.0	7	2.0
	6.0		22.0		6.0
	2.0		2.0		2.0
2	2.0	5	0.0		4.0
	0.0		8.0	8	3.5
	5.0		7.5		2.0
3	4.0	6	1.0		2.0
	2.0		6.0		

Table 2. Fe -.17%C. Annealing twin vestige analysis. Angles are those between surface shear directions and $\langle 110 \rangle_A$.

GRAINS	DEGREES	GRAINS	DEGREES	GRAINS	DEGREES
1	3.0	3	1.0	5	2.0
	0.0		1.0		1.0
	0.0		2.0		2.0
2	0.0	4	1.0		
	0.0		5.0		
	0.5		0.5		

Table 3. Fe- 6.0% Mn. Annealing twin vestige analysis. Angles are those between surface SHEAR normals and calculated austenite habit plane.

GRAINS	DEGREES	GRAIN	DEGREES	GRAIN	DEGREES
1	0.0	3	2.0	5	0.0
	2.0		5.0		3.0
	3.0		7.0		3.5
2	9.5	4	1.5		
	2.0		1.5		
	4.5		8.5		

Table 4. Fe - 6.0% Mn. Annealing twin vestige analysis. Angles are those between surface shear directions and $\langle 110 \rangle_A$.

Table 5: Pure Iron. Single Surface Trace Analysis. Angles given are those between normals to martensite substructure plates and indicated planes.

ZONE	DEGREES FROM					
	{100}	{110}	{111}	{112}	{145}	Calculated
{001}	41.5	3.5	3.5	1.0	3.0	1.0
{011}	2.0	2.0	33.0	22.0	8.0	11.0
	16.0	0.0	16.0	9.0	4.0	0.0
	39.5	2.0	10.0	2.0	2.0	2.0
{111}	9.5	7.0	22.0	6.5	1.0	0.0
	15.0	11.0	20.0	0.5	2.0	3.0
	15.0	11.0	16.0	0.5	2.0	3.0
	17.5	8.0	16.0	2.5	3.5	0.0
	19.0	6.5	11.0	4.0	4.0	2.0
{012}	20.5	8.0	7.0	1.0	2.0	1.0
{112}	37.0	1.0	18.0	7.5	0.0	3.0
	37.0	4.0	11.0	2.0	0.0	2.0
	17.0	0.0	10.0	0.0	5.0	10.0
	16.5	3.5	9.0	2.0	2.0	6.5
	15.0	6.0	8.0	3.0	1.0	3.5
{013}	16.0	10.0	0.0	0.5	1.0	1.0
{113}	17.0	9.0	20.0	6.0	0.0	0.0
	8.0	13.0	10.0	2.5	2.0	1.5
	25.0	9.0	8.0	2.0	2.0	0.0
{133}	8.0	2.0	20.0	10.0	6.0	11.0
	6.5	3.5	20.0	10.0	5.0	9.0
	7.0	5.0	20.0	10.0	4.0	8.5
	6.0	5.5	20.0	10.0	3.0	8.0
{135}	2.0	14.5	13.0	4.0	8.0	6.0

Table 6: Fe - .06% C. Single Surface Trace Analysis.
Angles given are those between normals to martensite substructure plates and indicated planes.

ZONE	DEGREES FROM					
	{100}	{110}	{111}	{112}	{145}	Calculated
{001}	42.5	2.5	2.0	2.0	4.0	1.5
{011}	39.0	4.0	16.0	4.0	3.0	1.0
{111}	23.0	1.0	27.0	8.5	2.0	2.0
	7.5	6.0	8.5	4.0	0.5	0.5
	10.5	7.5	12.0	5.0	0.5	2.0
	13.0	8.0	14.0	3.5	0.5	2.0
	15.5	10.0	18.0	0.5	0.0	4.0
{012}	21.0	5.5	7.5	2.0	2.0	2.0
	21.0	6.0	7.5	1.5	2.5	1.5
	18.0	6.0	6.5	3.5	0.5	0.0
	18.0	6.5	5.5	3.5	0.5	0.0
{112}	12.0	10.0	6.0	3.0	0.0	1.0
{113}	14.0	1.0	16.0	6.0	6.0	5.0
	16.0	3.5	18.0	7.0	3.0	3.0
	16.0	6.0	19.0	7.0	1.0	2.0
	17.5	8.5	20.0	7.0	2.0	1.0
	25.0	8.0	11.0	2.0	0.0	1.0
{123}	32.0	3.0	17.0	1.0	3.5	1.0
{133}	5.0	6.0	22.0	0.0	3.0	0.0
	34.0	4.0	12.0	10.0	2.0	0.0
{014}	10.5	2.0	6.0	8.0	3.0	0.0
{115}	15.0	9.5	3.5	4.0	2.0	1.0
{135}	3.5	16.0	9.5	3.5	6.0	6.0
	12.0	11.0	6.0	3.0	0.0	1.0
	13.0	5.5	3.0	6.5	1.0	1.0
	12.0	7.0	0.0	4.5	0.5	1.0

Table 7: Fe - .17% C. Single Surface Trace Analysis. Angles given are those between normals to martensite substructure plates and indicated planes.

ZONE	DEGREES FROM					
	{100}	{110}	{111}	{112}	{145}	Calculated
{001}	38.5	6.5	6.0	4.0	0.5	3.0
	35.5	9.5	7.5	5.5	3.5	5.5
	24.0	16.0	16.5	2.5	6.0	2.5
{111}	22.0	2.0	26.0	8.0	2.5	8.5
	19.5	5.5	23.0	5.0	2.0	3.5
	18.5	6.0	22.0	4.0	3.0	2.0
	13.0	9.0	15.5	2.0	3.0	0.0
	14.0	9.5	19.0	1.0	2.0	3.5
	14.0	10.5	17.5	0.0	0.0	2.0
{012}	24.0	1.0	0.0	10.0	4.0	7.0
	26.0	2.0	2.0	8.0	2.0	4.5
	30.0	4.0	4.0	4.5	1.0	2.0
	6.0	3.0	24.0	12.0	3.0	1.0
{112}	12.0	9.0	7.5	5.0	1.0	0.0
{122}	16.0	6.0	4.5	3.0	2.5	0.0
	10.0	7.0	16.0	4.0	0.0	5.0
	8.0	10.0	16.0	4.0	1.0	3.0
{113}	12.0	5.5	14.0	1.5	0.5	4.0
	11.0	6.0	14.0	1.5	0.5	4.0
{123}	18.0	6.0	4.5	3.0	1.0	1.0
{133}	30.5	0.5	9.0	3.5	1.0	3.0
{115}	15.0	12.0	0.0	0.0	1.0	1.5
	3.0	9.0	6.0	3.5	2.0	4.5
{135}	13.0	4.5	4.0	8.0	2.0	3.0
	18.0	6.0	3.5	4.5	0.5	2.0
{353}	13.0	7.5	14.0	0.5	2.0	2.5
{317}	4.0	3.0	25.0	14.0	0.0	3.5

Table 8: Fe - 6.0% Mn. Single Surface Trace Analysis.
Angles given are those between normals to martensite substructure plates and indicated planes.

ZONE	DEGREES FROM					
	{100}	{110}	{111}	{112}	{145}	Calculated
{001}	16.5	13.0	24.0	9.0	1.0	0.5
	44.0	2.0	0.5	0.0	5.0	3.0
	39.5	6.0	4.0	2.5	1.0	2.0
{011}	35.0	0.5	18.0	0.5	0.0	4.0
	35.0	0.5	18.0	0.5	0.0	4.0
	35.0	0.5	18.0	0.5	0.0	4.0
	40.0	3.0	15.0	2.5	4.0	0.0
	19.0	14.0	10.0	8.0	3.0	2.5
	19.0	14.0	10.0	8.0	3.0	2.5
{111}	23.5	0.5	29.0	10.0	3.0	8.5
	23.5	0.5	29.0	10.0	3.0	8.5
	21.5	3.0	26.0	8.0	1.0	6.5
	20.0	4.5	24.0	6.0	0.5	4.5
	19.0	7.5	21.5	4.0	3.0	2.0
	17.0	10.0	19.0	2.0	2.0	1.0
{012}	12.5	10.0	8.0	2.0	1.0	0.0
	26.0	4.0	3.5	4.5	1.0	0.0
	26.0	2.0	10.5	6.0	2.0	0.5
{112}	32.5	1.0	20.0	3.0	1.0	0.0
	18.0	10.0	20.0	10.0	1.0	1.5
{122}	6.0	10.0	16.0	2.5	0.0	2.0
	14.0	0.0	16.0	6.0	7.0	7.0
{113}	18.0	4.0	14.5	3.5	2.0	6.5
	24.0	2.0	12.0	4.0	0.5	0.5
	24.0	4.0	10.0	3.0	0.5	0.5
{133}	33.0	2.0	12.0	2.0	0.5	2.0
{135}	28.0	6.5	11.0	2.5	0.5	2.0

Table 9: Fe - 1.7% Si - 7.83% Mn. Single Surface Trace Analysis. Angles given are those between normals to martensite substructure plates and indicated planes.

ZONE	DEGREES FROM					
	{100}	{110}	{111}	{112}	{145}	Calculated
{001}	44.5	0.0	0.0	0.0	5.5	3.0
	42.5	2.5	2.0	1.0	3.5	1.0
	41.0	4.0	3.0	2.0	2.5	0.5
	37.5	7.0	6.0	4.0	1.0	4.0
{011}	4.0	8.0	28.0	18.0	2.0	7.0
	3.0	6.0	30.0	20.0	4.0	9.0
	2.0	4.0	32.0	22.0	6.0	11.0
	18.0	25.0	14.5	0.0	5.0	11.0
	33.0	4.0	15.0	4.0	3.0	0.0
	36.0	0.5	20.0	0.5	0.0	3.5
{111}	23.5	1.0	27.0	9.0	3.0	1.0
	22.5	3.0	26.5	8.5	2.0	6.5
	20.5	7.0	23.5	5.5	1.5	3.0
	15.5	11.0	28.5	0.0	0.0	2.0
	13.0	8.0	14.0	3.5	4.0	1.5
	10.5	7.5	12.0	5.0	3.0	7.5
{012}	20.0	3.0	9.5	6.0	3.0	0.5
	21.0	5.0	8.0	2.5	1.0	2.5
	22.0	6.5	15.0	1.5	0.5	0.0
{112}	12.5	10.0	7.0	4.5	0.5	0.0
{013}	18.0	1.0	8.5	10.0	3.0	4.5
	11.0	5.0	13.5	5.0	1.0	6.0
{113}	13.0	1.0	15.0	2.0	4.0	6.5
	18.0	12.0	22.0	8.0	2.0	0.0
	25.0	11.0	5.5	4.0	0.5	4.0
	26.0	1.0	13.5	5.5	1.0	6.0
	26.0	0.0	14.0	4.5	2.0	0.0
{115}	15.0	7.0	4.0	4.5	2.0	1.0
	15.0	7.5	3.5	4.0	2.5	1.0
{133}	30.0	4.0	13.0	0.0	2.0	1.0
{135}	4.0	15.0	10.0	2.0	6.0	3.0
{353}	11.5	9.0	9.5	3.0	2.5	2.0

Table 10: Fe - 10.79% Ni. Single Surface Trace Analysis. Angles given are those between normals to martensite substructure plates and indicated planes.

ZONE	DEGREES FROM					
	{100}	{110}	{111}	{112}	{145}	Calculated
{001}	35.0	7.5	8.0	5.5	3.0	5.5
	42.0	2.5	2.0	1.5	4.0	2.0
	40.5	4.0	3.5	2.5	2.0	0.0
	39.0	5.5	4.5	3.0	1.0	2.0
	35.0	7.5	8.0	5.5	3.0	5.5
	31.0	14.0	11.0	4.0	7.0	8.0
{011}	29.5	9.5	10.5	4.0	0.0	1.0
{111}	23.5	3.0	27.0	8.5	2.0	7.0
	22.5	3.0	26.0	8.0	1.0	6.0
	20.0	6.0	22.0	4.0	3.0	3.0
	17.5	10.0	19.0	1.0	3.0	1.0
{012}	20.0	2.0	10.0	5.5	1.0	0.0
	20.0	3.5	9.5	4.0	0.0	1.5
	20.0	4.0	9.0	3.5	0.5	2.0
	22.0	8.0	7.0	0.5	3.0	0.0
	23.0	4.0	4.0	4.5	0.5	2.0
{112}	13.5	8.0	8.0	4.0	3.0	2.0
{122}	12.0	16.0	0.0	5.0	0.0	1.5
{013}	12.0	14.0	0.5	3.5	0.5	2.0
{113}	3.5	5.5	3.0	1.0	0.5	2.0
	3.5	7.5	4.0	1.0	1.0	3.0
	10.0	6.5	12.0	0.0	2.0	2.0
{133}	13.0	14.0	4.0	1.5	5.5	2.0
{115}	8.5	3.0	20.0	8.5	4.0	2.5

Table 11. Single Surface Trace Analysis
Angles given are those between directions of martensite substructure plates and $\langle 111 \rangle_M$.

ZONE	PURE IRON	Fe-.06 C	Fe-.17 C	Fe-6.0 Mn	Fe-1.7 Si 7.83 Mn	Fe-10.79 Ni
{011}	2.5	2.5	6.0	4.0	0.5	2.0
			8.5	1.0	2.0	3.5
			18.0	22.5	3.5	5.0
					6.0	8.0
						11.5
{011}	1.0	4.0		4.0	0.5	10.0
	4.0			1.0	4.0	
	19.5			15.5	15.0	
				16.5	2.0	
					3.0	
					4.5	
{111}	6.0	6.0	2.0	1.5	0.5	2.0
	8.0	8.0	5.5	3.5	1.5	3.5
	10.0	10.0	6.5	3.5	5.0	6.5
	10.0	10.0	10.5	5.0	10.0	9.5
	18.0	18.0	13.0	8.0	13.5	
			9.0	10.0	16.0	
{012}	1.0	0.0	6.0	24.0	4.0	3.5
		1.5	10.0	7.0	0.5	2.0
		9.5	12.5	4.0	4.5	1.5
		10.5	7.0			2.0
						7.0
{112}	3.0	1.0	1.0	7.0	0.5	2.0
	4.0			3.0		
	3.0					
	6.0					
	9.0					
{122}			16.5	1.0		8.0
			2.0	7.0		
			2.5			
{013}	6.0				1.5	4.0
{113}	3.0	15.5	8.0	2.0	9.0	7.0
	2.0	18.0	9.0	3.0	13.0	8.0
	20.0	20.0		11.5	20.0	9.5
		22.0			6.0	
		2.0			0.0	
					1.0	
{123}		2.0	5.0			
{133}	5.0	2.0	2.5	0.0	1.0	2.5
	6.0	1.0				
	6.5					
{014}		4.0				
{115}		10.5	2.0		1.5	8.5
			6.5		2.5	
{135}	1.0	7.0	6.5	19.0	7.0	
	4.0	6.0	6.5			
		10.0				
		7.0				
{353}			10.0		10.0	

	$(111)_A[\bar{1}\bar{1}2]_A$		$(100)_A[010]_A$	
V_I	g	S	g	S
1.00	.251131	.231575	.231566	.466238
1.03	.275677	.224947	.251413	.484876
1.04	.284290	.222686	.257906	.488759
1.08866	.353555	.142965	.288672	.516840

Table 12. Calculated values of dislocation shear (g) and shape deformation (S) for two choices of the inhomogeneous shear.

	$(111)_A[\bar{1}\bar{1}2]_A$		$(100)_A[010]_A$	
V_I	$(111)_A : (011)_M$	$[0\bar{1}1]_A : [1\bar{1}1]_M$	$(111)_A : (011)_M$	$[0\bar{1}1]_A : [1\bar{1}1]_M$
1.00	4.30°	0.78°	6.08°	0.95°
1.03	3.50°	0.50°	6.60°	0.72°
1.04	3.20°	0.48°	6.70°	0.62°
1.08866	0.0°	0.0°	7.40°	0.0°

Table 13. Calculated parallelism between indicated shear elements for two choices of the inhomogeneous shear.

	$(111)_A[\bar{1}\bar{1}2]_A$		$(100)_A[010]_A$	
V_I	H_A	H_M	H_A	H_M
1.00	-.585345	-.665241	.584838	-.035818
	.470595	-.179279	.521031	.620593
	.660242	.724813	.621682	.783283
1.03	-.634885	-.715669	.602539	-.040314
	.479003	-.214413	.531538	.643951
	.606198	.664714	.595327	.764005
1.04	-.653270	-.732110	.608047	-.041695
	.479698	-.228936	.534671	.649478
	.585768	.641558	.586860	.759230
1.08866	-.816495	-.816492	.632453	-.048919
	.408239	-.408250	.547721	.681372
	.408256	.408246	.547725	.730303

Table 14. Calculated direction cosines for austenite (H_A) and martensite (H_M) habit planes for two choices of the inhomogeneous shear.

	$(111)_A[\bar{1}\bar{1}2]_A$		$(100)_A[010]_A$	
V_I	H_A : {111}	H_M : {145}	H_A : {111}	H_M ; {145}
1.00	7.77°	4.08°	4.17°	6.83°
1.03	6.75°	5.43°	3.27°	6.73°
1.04	7.12°	5.03°	3.22°	6.75°
1.08866	19.47°	19.10°	3.97°	7.45°

Table 15: Calculated angles between given planes for two choices of the inhomogeneous shear.
$H_A \equiv$ Austenite habit plane
$H_M \equiv$ Martensite habit plane

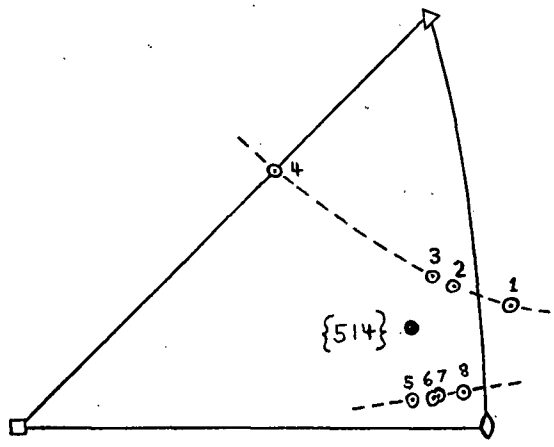

Fig. 1: Variation of Calculated Martensite Habit Plane with V_I.

	Inhomogeneous Shear System	
V_I	$(111)_A[\bar{1}\bar{1}2]_A$	$(100)_A[010]_A$
1.00	1	5
1.03	2	6
1.04	3	7
1.08866	4	8

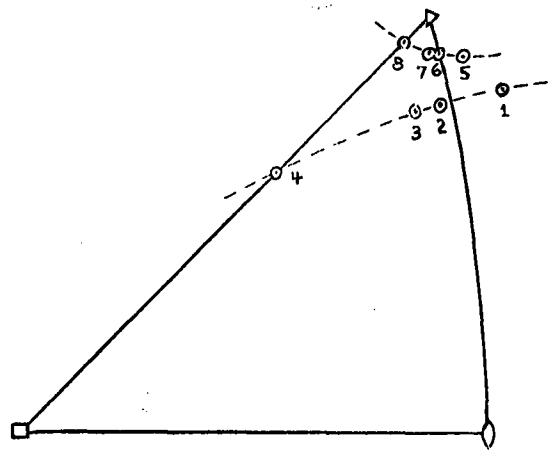

Fig. 2: Variation of Calculated Austenite Habit Plane with V_I.

	Inhomogeneous Shear System	
V_I	$(111)_A[\bar{1}\bar{1}2]_A$	$(100)_A[010]_A$
1.00	1	5
1.03	2	6
1.04	3	7
1.08866	4	8

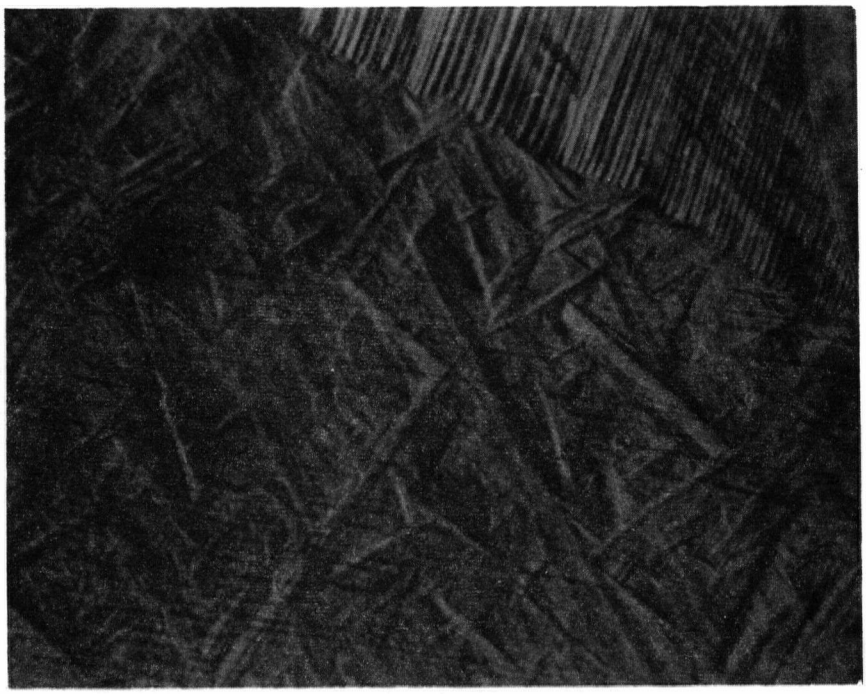

Fig. 3. Pure Iron. Martensite Surface Shears. 1060 X.

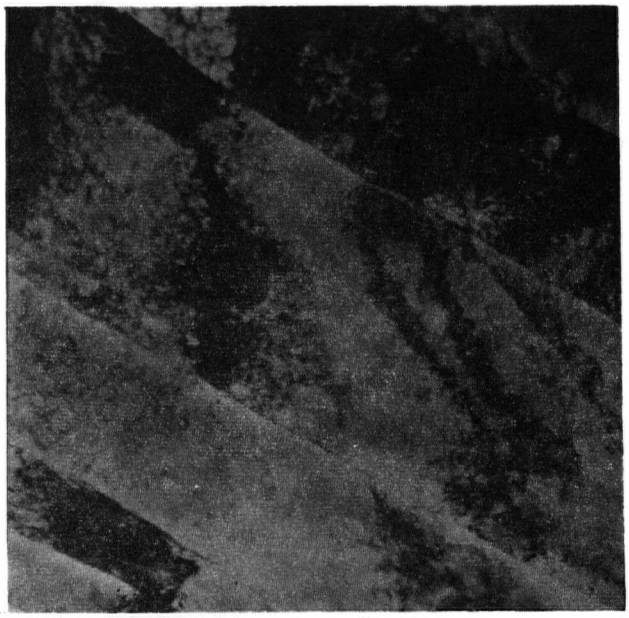

Fig. 4. Pure Iron. Martensite Substructure. 29000 X.

Fig. 5. Fe - 0.06% C. Martensite Surface Shears. 530 X.

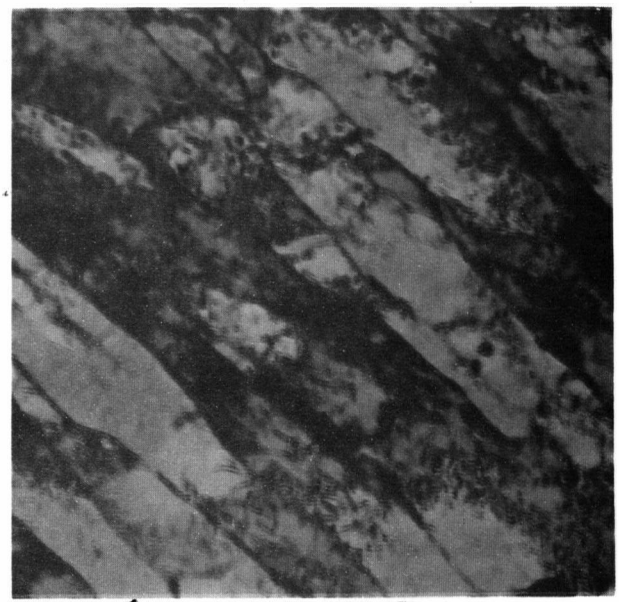

Fig. 6. Fe - 0.06% C. Martensite Substructure. 29000 X.

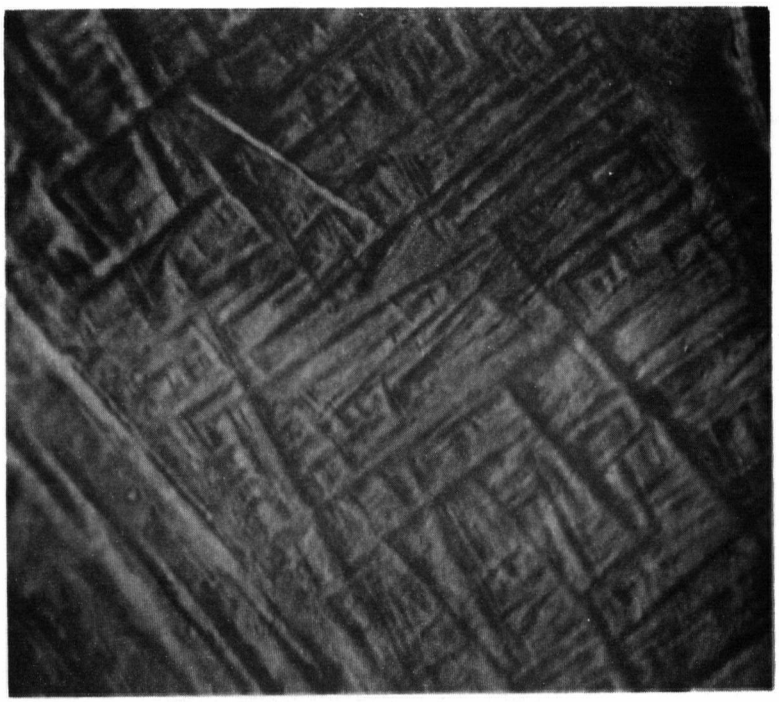

Fig. 7. Fe - 0.17% C. Martensite Surface Shears. 1430 X.

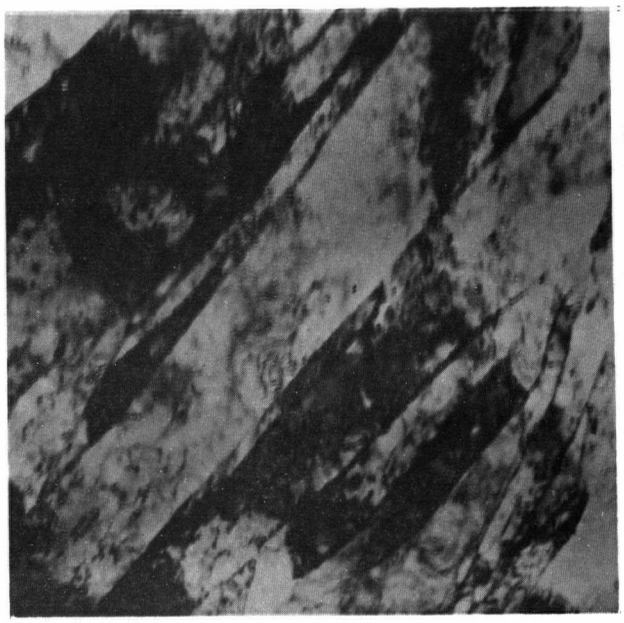

Fig. 8. Fe - 0.17% C. Martensite Substructure. 29000 X.

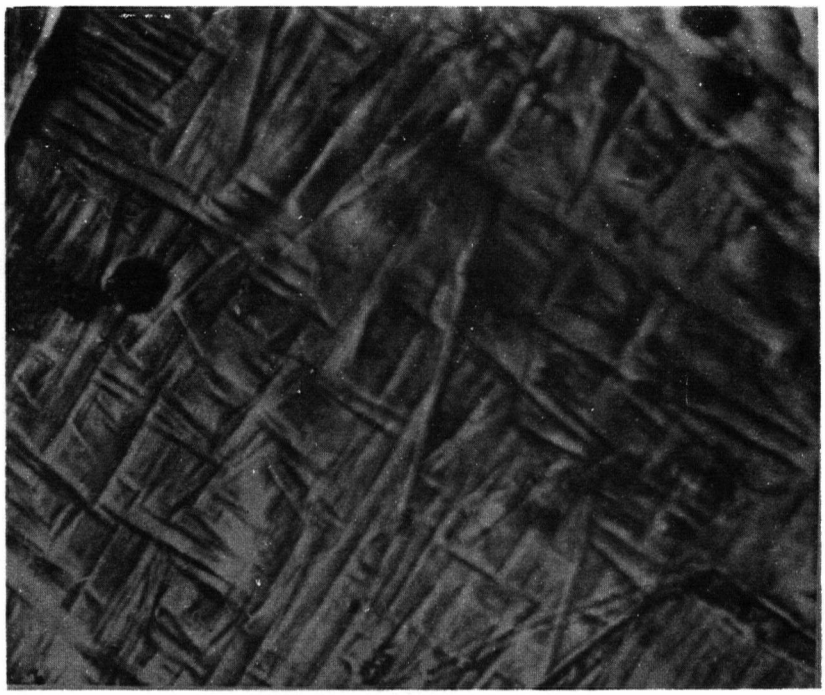

Fig. 9. Fe - 6.0% Mn. Martensite Surface Shears. 1100 X.

Fig. 10. Fe - 6.0% Mn. Martensite Substructure. 29000 X.

Fig. 11. Fe - 1.7% Si - 7.83% Mn. Martensite Surface Shears. 1060 X.

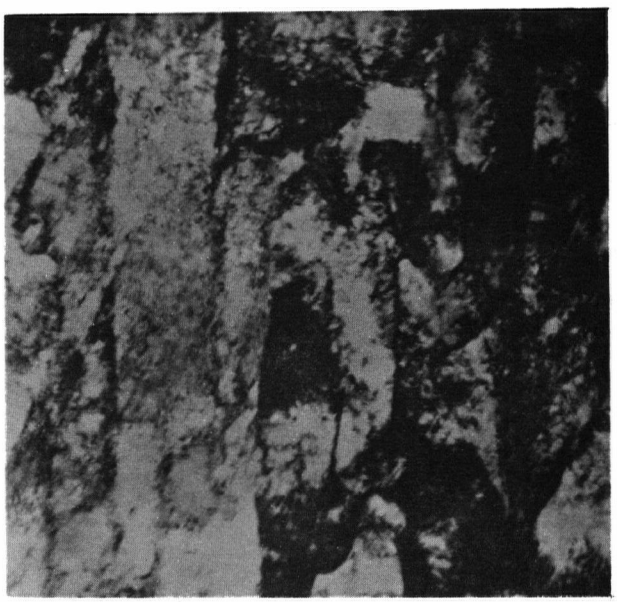

Fig.12. Fe - 1.7% Si - 7.83% Mn. Martensite Substructure. 29000 X.

Fig. 13. Fe - 10.79% Ni. Martensite Surface Shears. 1060 X.

Fig. 14. Fe - 10.79% Ni. Martensite Substructure. 29000 X.

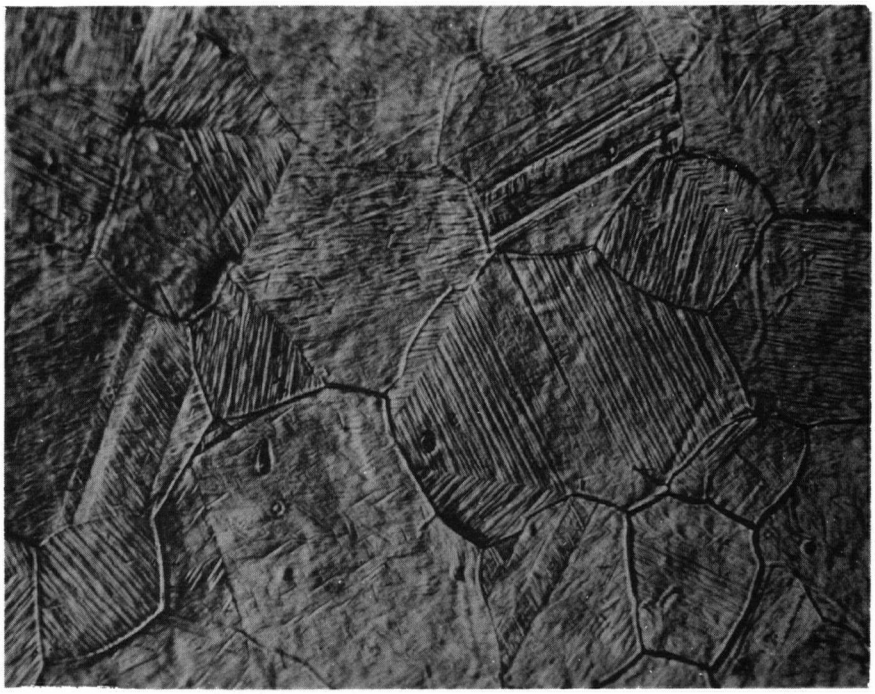

Fig. 15. Fe - .17% C. 200X.
Austenite Annealing Twin Vestiges within prior austenite grains.

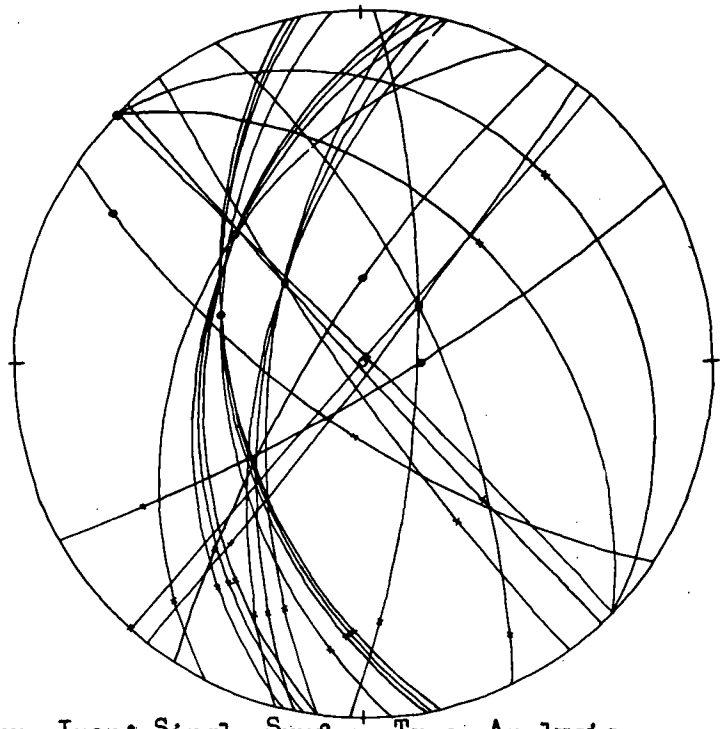

Fig. 16. Pure Iron: Single Surface Trace Analysis
Standard (001) Cubic Projection.
⊙ Zone axis of plane of image
× Direction of substructure plates in image plane

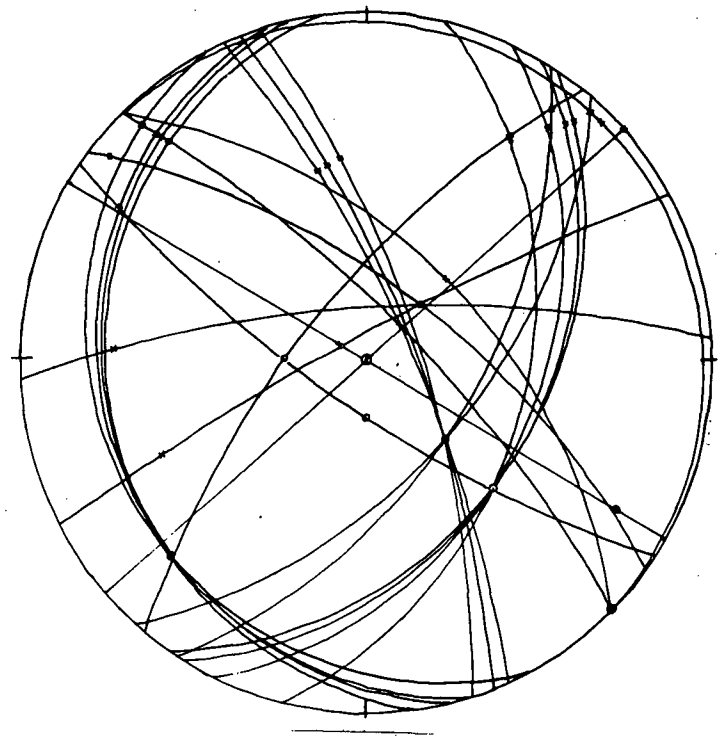

Fig. 17. Pure Iron : Single Surface Trace Analysis.
Standard (001) Cubic Projection.
⊙ Zone axis of plane of Image
× Direction of Normal to substructure plates in Image Plane.

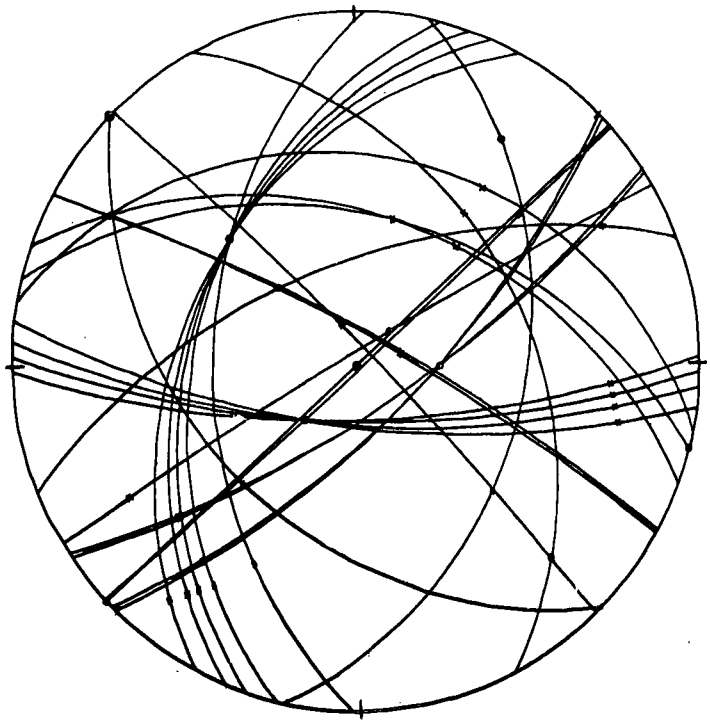

Fig. 18. Fe -.06% C. Single Surface Trace Analysis.
Standard (001) Cubic Projection
⊙ Zone axis of plane of Image.
✗ Direction of Substructure plates in Image Plane.

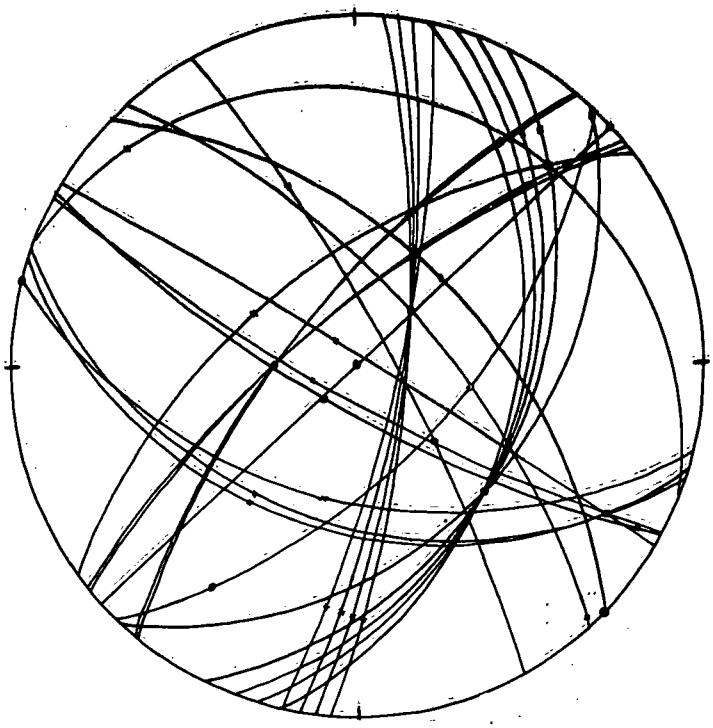

Fig. 19. Fe - .06% C. Single Surface Trace Analysis.
Standard (001) Cubic Projection.
⊙ Zone axis of Plane of Image.
✗ Direction of Normal to Substructure plates in Image Plane.

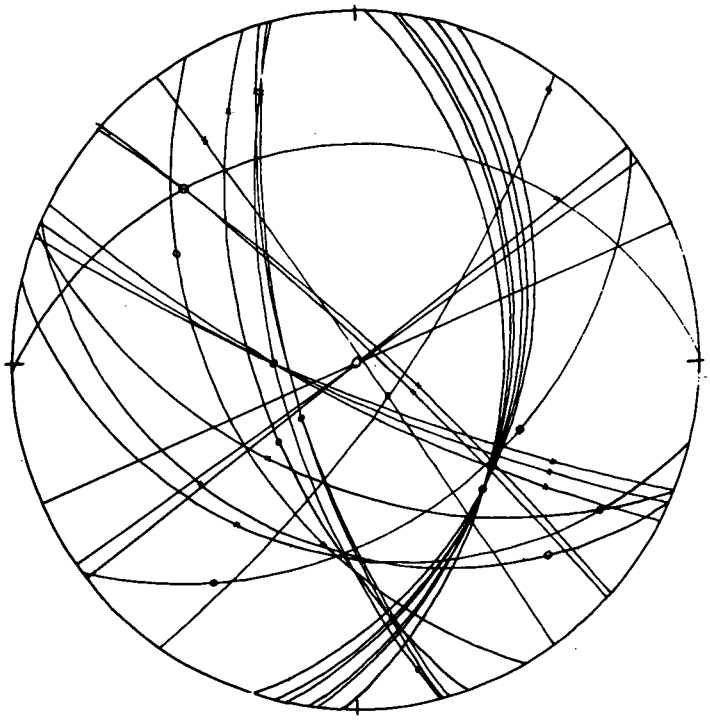

Fig. 20. Fe - .17% C. Single Surface Trace Analysis.
Standard (001) Cubic Projection.
⊙ Zone axis of Plane of Image.
× Direction of Substructure plates in Image Plane.

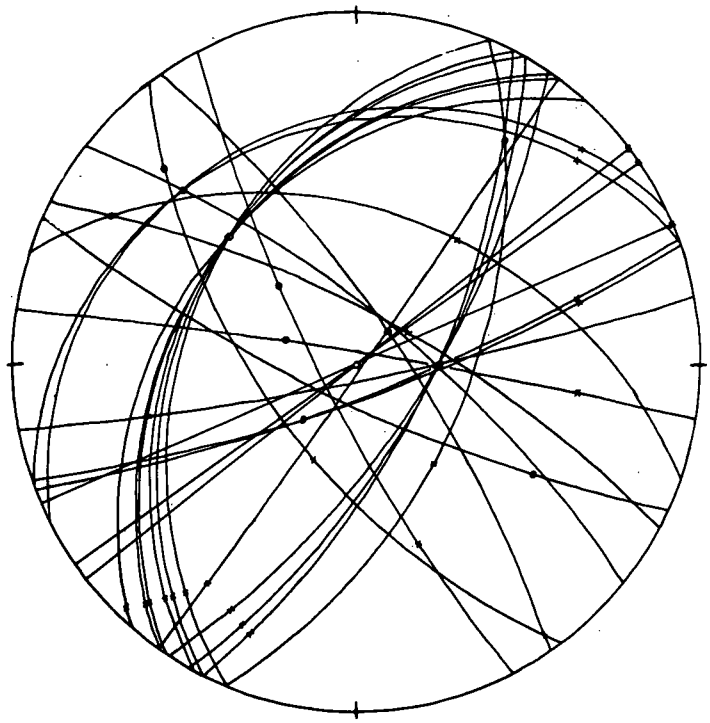

Fig. 21. Fe - .17% C. Single Surface Trace Analysis.
Standard (001) Cubic Projection.
⊙ Zone axis of Plane of Image.
× Direction of Normal to Substructure plates in Image Plane.

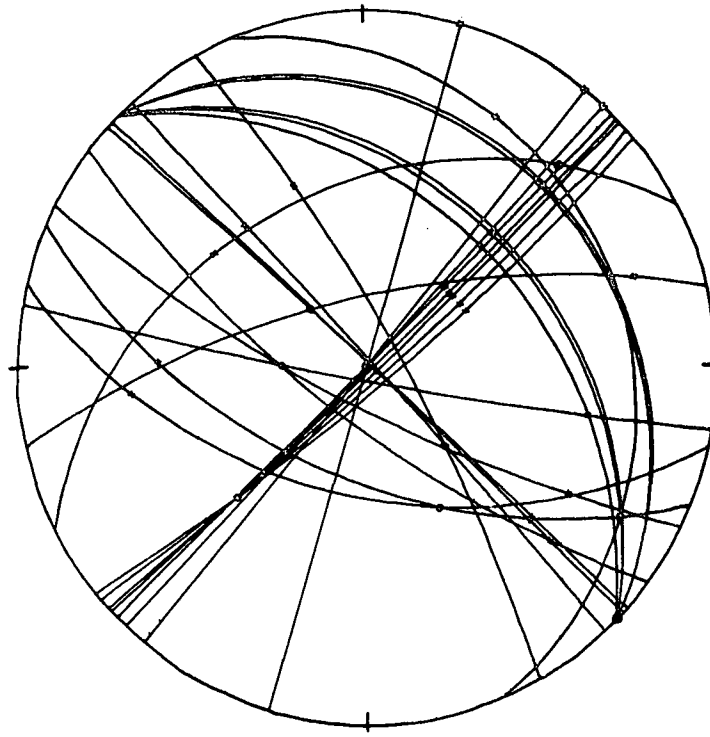

Fig. 22. Fe - 6.0% Mn. Single Surface Trace Analysis.
Standard (001) Cubic Projection.
⊙ Zone axis of Plane of Image.
X Direction of Substructure plates in Image Plane.

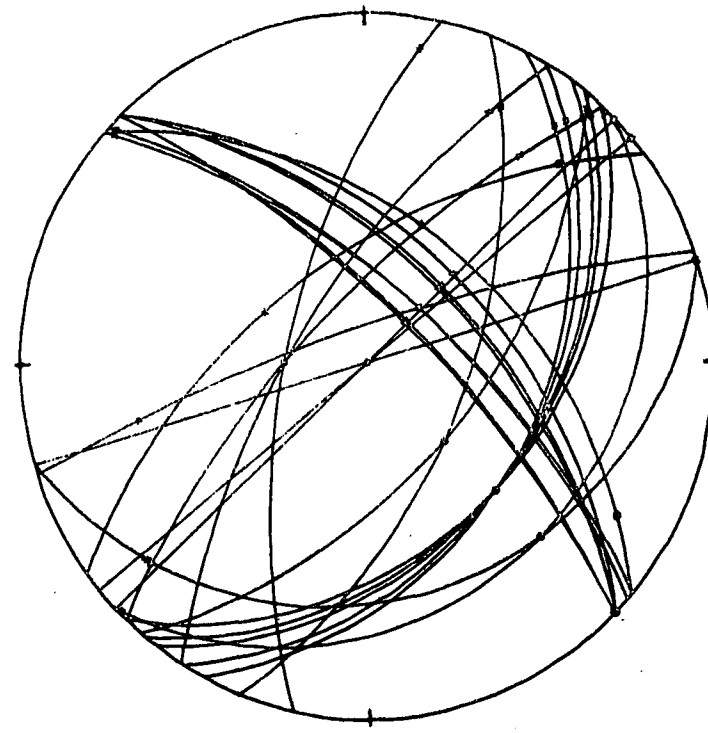

Fig. 23. Fe - 6.0% Mn. Single Surface Trace Analysis.
Standard (001) Cubic Projection.
⊙ zone axis of Plane of Image.
X Direction of Normal to Substructure plates in Image Plane.

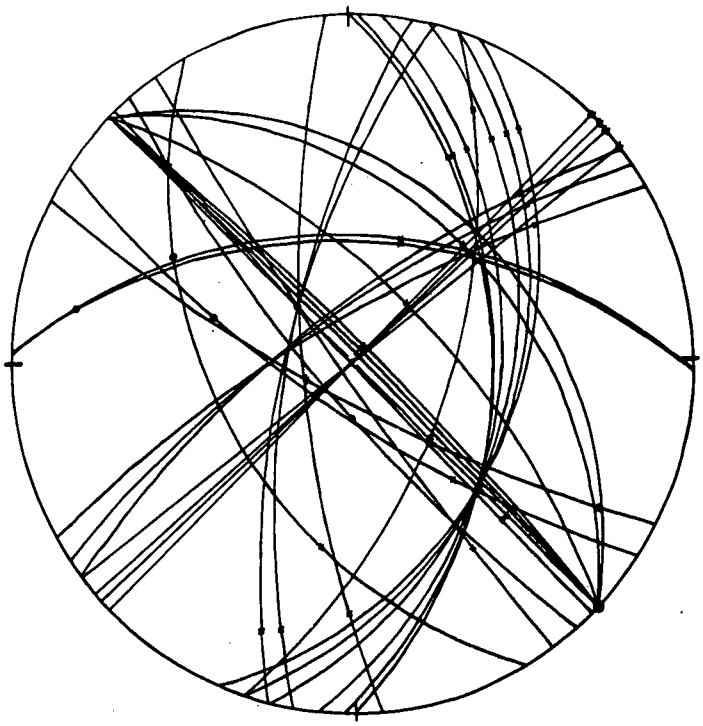

Fig. 24. Fe - 1.7% Si - 7.83% Mn. Single Surface Trace Analysis.
Standard (001) Cubic Projection.
⊙ Zone axis of Plane of Image.
x Direction of Substructure plates in Image Plane.

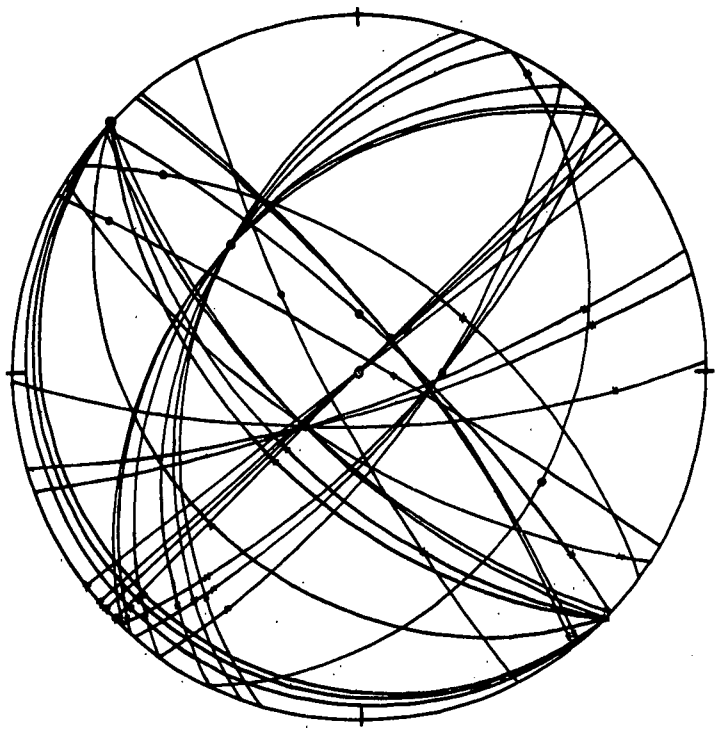

Fig. 25. Fe - 1.7% Si - 7.83% Mn. Single Surface Trace Analysis.
Standard (001) Cubic Projection.
⊙ Zone axis of Plane of Image.
x Direction of Normal to Substructure plates in Image Plane.

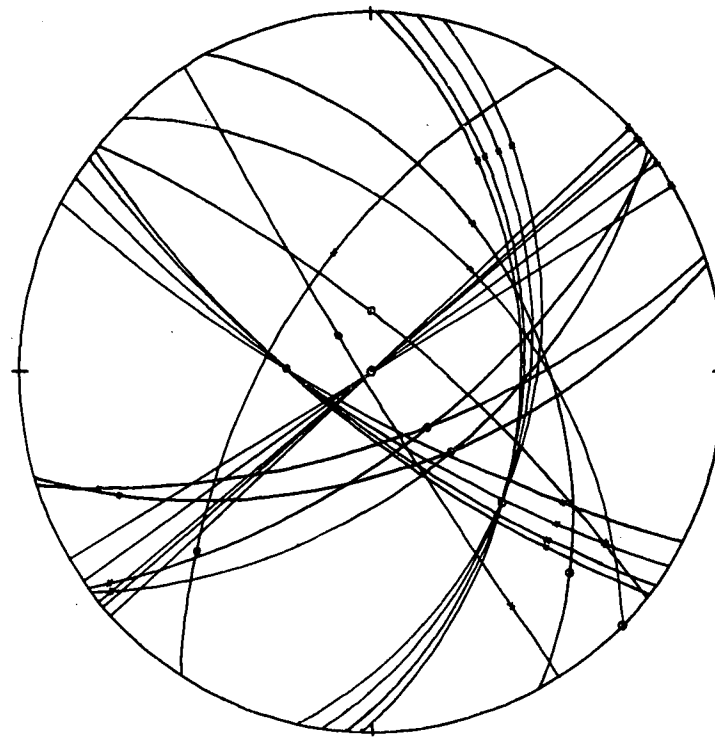

Fig. 26. Fe - 10.79% Ni. Single Surface Trace Analysis.
Standard (001) Cubic Projection.
⊙ Zone axis of Plane of Image
× Direction of Substructure plates in Image Plane.

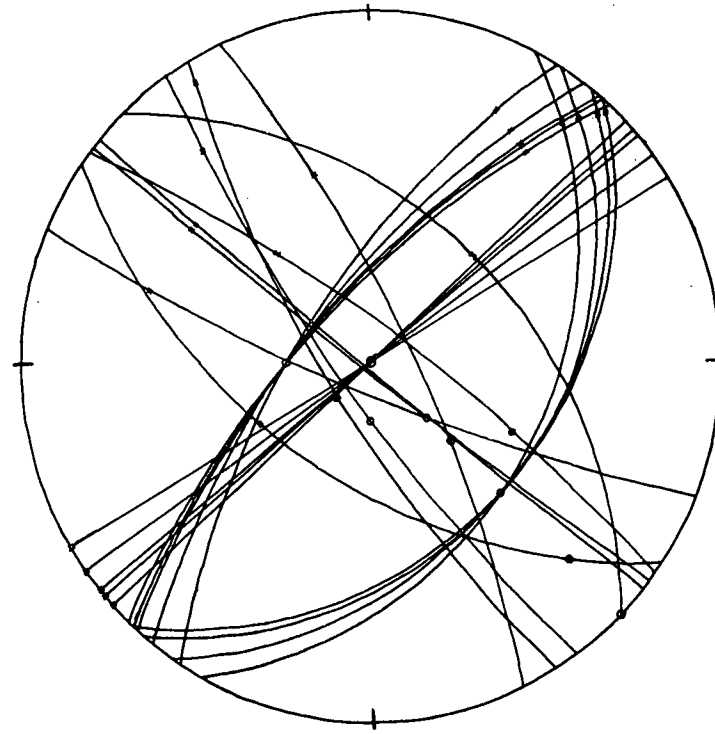

Fig. 27. Fe - 10.79% Ni. Single Surface Trace Analysis.
Standard (001) Cubic Projection.
⊙ Zone axis of Plane of Image.
× Direction of Normal to Substructure Plates in Image Plane.

DISCUSSION OF RESULTS

SURFACE SHEARS

The formation of surface shears is used universally throughout the the martensite literature as an important criterion as to whether or not a martensite transformation has taken place. All six of the alloys studied were found to form surface shears and furthermore the shears in all alloys appear alike which suggests that the mechanism of the martensite transformation is similar. The shears were found contained within thermally etched boundaries which are assumed to be those of the high temperature austenite phase (8). Owen, Wilson, and Bell (8) in their study of the massive martensite structures in Fe-Ni state that they found no more than 4 different orientations to the surface shears within any volume formed from an austenite grain. This led them to believe that the habit plane is $\{111\}_A$. In this study 4 is the largest number of unique shears which regularly appear, but with diligent observation it is possible to find martensite volumes which have formed from austenite grains with 5 or more unique orientations. From a study of the photograph which Owen, Wilson and Bell present as an example of the surface shears in Fe-Ni it would appear that they came to their conclusion possibly because their austenite grain size was too small, hence not allowing all possible shear orientations to form. From the study of the relative numbers of time in which 4 or 5 orientations appear it would seem that the austenite habit plane is close to $\{111\}_A$.

The percentage of a grain which has transformed martensitically depends on the temperature of the alloy relative to the M_s and M_f temperatures. As a speciman is quenched a small portion is transformed instantaneously to martensite as soon as the M_s temperature is reached. It now may well be that the orientation of all subsequent martensite formed as the temperature is dropped from M_s to M_f is determined by the first crystals formed at M_s.

From strain energy considerations it may also be that only a small number of the possible different orientations will manifest themselves once the first crystals are formed at M_s. Hence possibly the reason for seldom observing more than 4 different orientations to the shear traces. If this were the case then the fact that only 4 orientations are usually observed would not necessarily imply a habit plane close to $\{111\}_A$.

The appearance of austenite annealing twin vestiges in these alloys complicates the counting of the number of shear orientations within a volume formed from an austenite grain, but does open up the possibility of being able to predict the austenite habit plane. Greninger and Troiano (4) investigated the low carbon martensites by a study of the austenite twin vestiges and observed a $\{111\}$ austenite habit plane. With this in mind it was decided to study the twin vestiges in the Fe - .17% C and Fe - 6.0% Mn alloys, which are representative of those examined in this thesis. The twin vestiges gave the orientation of the grain relative to the austenite axis and hence it was possible to compare the surface shear normals and directions to specific crystallographic directions. In tables 1 and 3 can be seen the extremely close agreement between the calculated austenite habit plane (7.12 degrees from $\{111\}_A$) and the great circles drawn between the directions normal to the surface shears and the pole of the grain. Identical results have also been observed by work within the department (30) on the Fe-- 4.8% Cu martensite.

From tables 2 and 4 it can be seen that the shear traces are in the majority of cases consistent with the directions $\langle 110\rangle_A$. However the fact that there are a significant number of shear traces whose directions are not consistent with $\langle 110\rangle_A$ would appear to rule out the possibility that the martensite crystals are needles whose axis is along $\langle 110\rangle_A$. Plates which are elongated in a direction close to $\langle 110\rangle_A$ in the habit plane could though be consistent with the data in Tables 2 and 4.

ELECTRON MICROSCOPY:

From the results of the single surface trace analysis it is not possible to state the martensite habit plane with assurance. It is possible though to say that the martensite habit plane is not a plane of low indices, because from the tables 5 to 10 it can be seen that for the martensite habits $\{100\}$, $\{\overset{110}{\cancel{100}}\}$, $\{111\}$ and $\{112\}$ a large number of the traces are greater than 5 degrees (the generally accepted criterion) away. A single surface trace analysis is to a large extent a statistical method in that it can only hope to predict a given habit plane when a large number of traces (i.e. 25 - 30) are used, and when all these traces are consistent with a plane whose poles are grouped into a few discrete regions.

It does appear though that the trace analyses on all 6 alloys are consistent with the $\{145\}_M$ and calculated (using $(111)_A[\bar{1}\bar{1}2]_A$ with $V_I = 1.04$) habit planes. The $\{145\}_M$ habit plane gives a slightly better fit. But what must be realized is that the poles of the $\{145\}$ plane are so situated on the stereogram that it is possible to draw a number of random traces (i.e. 30) and still have no trace deviate by more than 8 - 9 degrees from a $\{145\}$ pole. The poles calculated using $(111)_A[\bar{1}\bar{1}2]_A$ with $V_I = 1.04$ are distributed similarly to the $\{145\}_M$ poles but do not cover the stereogram as thoroughly. Hence possibly the reason why the fit is not quite as good as for $\{145\}$.

In summary, it can be seen from Figs. 16, 18, 20, 22, 24, 26 that the poles of the martensite habit plane must be well distributed around the stereogram. Such a distribution is given by $\{145\}$ and by the plane calculated using $(111)_A[112]_A$ with $V_I = 1.04$ in the WLR theory.

The directions parallel to the martensite needles were not found to be consistent with $\langle 111\rangle_M$ directions as found by Kelly and Nutting (6) in low C steels. As can be seen from Table 11 it would be possible to conclude that the traces are parallel to $\langle 111\rangle_M$ if a sufficient number of traces were

not examined, and it is suspected that this is the case with the work of Kelly and Nutting. Bowles (5) believed that the observed $\{111\}_A$ habit plane was composed of laths parallel to $\langle 101\rangle_A$ directions and hence must be considered only a pseudo habit plane. If an orientation relationship close to Kurdjumov-Sachs is valid then $\langle 101\rangle_A$ is approximately parallel to $\langle 111\rangle_M$. But this work has shown that martensite crystals do not have a common direction of $\langle 111\rangle_M$. Hence a true habit plane close to $\{111\}_A$ is a possibility.

The experimental evidence is inconsistent with the possibility of the martensite crystals being needles as no common direction was found. The fact that a common plane was identified though does not rule out the possibility that the plates may be elongated in a given direction within the habit plane.

CALCULATIONS:

To explain theoretically the experimental results the following must be predicted by the theory:

(1) An austenite habit plane close to $\{111\}_A$

(2)A martensite habit plane close to $\{145\}_M$

(3) An orientation relationship close to Kurdjumov - Sachs.

Items (1) and (2) are the results of the experimental work while item (3) is assumed as the Kurdjumov - Sachs relationship is found in Fe-Ni massive martensite (8) and in low carbon martensites (26).

Also the theory must predict relatively small values of g, the slip shear, and S, the macroscopic shear, from the use of slip systems which are equivalent to those normally found in either of the two phases.

It has been possible to find two slip systems which when applied to the WLR theory are able to satisfy the above requirements; they are $(111)_A[\bar{1}\bar{1}2]_A$ and $(100)_A[010]_A$.

Crocker and Bilby (21) by use of computer programs, studied thoroughly the problem of predicting the $\{111\}_A$ habit plane using the general theory of Bullough and Bilby. They came to the conclusion that only the shear mode $(1\bar{1}0)_M[\bar{1}10]_M$ or the equivalent mode $(110)_M[1\bar{1}0]_M$ were possibilities.

Hence it was decided to investigate using the WLR theory the system $(110)_M[\bar{1}10]_M$ which is equivalent to $(100)_A[010]_A$ by the correspondence matrices. The calculated values of "g" and "S" are given in table 12. If it is realized that the magnitude of "g" can range from $0.2 \rightarrow 1.7$ and of "S" from $0.14 \rightarrow 1.9$ depending on the shear mode, then those values predicted using $(100)_A[010]_A$ are relatively low. The significance of the magnitudes of "g" and "S" are not well understood; but it seems reasonable that "g", a measure of the amount of dislocation slip, and "S", a measure of the deformation necessary to accomodate the change in macroscopic shape will be important factors in determining the energy associated with the formation of a martensite plate. The parameter V_1 will be defined farther on.

In table 13 are given the calculated angles between certain planes and directions for the $(100)_A[010]_A$ system. The orientation relationship can be seen to be close to Kurdjumov - Sachs. From table 15 it can be seen that H_A is $3 \rightarrow 4^o$ from $\{111\}_A$ while H_M is ~ 7 degrees from $\{145\}_M$. Hence we see that the system $(100)_A[010]_A$ satisfies the criterions.

Otte (20) has also investigated the commonly observed slip systems in the austenite and martensite but again, as with the work of Crocker and Bilby, he only goes as far as calculating the austenite habit plane. If we allow a greater deviation from $\{111\}_A$ than have Crocker and Bilby the system $(111)_A[\bar{1}\bar{1}2]_A$ is also found to fit the previously stated criterions. It predicts values of "g" (table 12) which are approximately as those for $(100)_A[010]_A$ but the "S" values are only half those for $(100)_A[010]_A$. Furthermore the orientation relationship (table 11) is closer to Kurdjumov - Sachs than for $(100)_A[010]_A$. $(111)_A[\bar{1}\bar{1}2]_A$ predicts an austenite habit plane

about 7 degrees (table 15) from $\{111\}_A$ and a martensite habit plane within 5 degrees of $\{145\}_M$.

By the correspondence matrices (see Appendix I) the systems $(100)_A[010]_A$ and $(111)_A[\bar{1}\bar{1}2]_A$ can be shown to be equivalent respectively to $(110)_M[\bar{1}10]_M$ and $(011)_M[0\bar{1}\bar{1}]_M$. Observing that:

$$a[\bar{1}10] = a/2[\bar{1}11] + a/2[\bar{1}1\bar{1}]$$
$$a[0\bar{1}1] = a/2[\bar{1}11] + a/2[1\bar{1}1]$$

it is seen that systems $(110)_M[\bar{1}10]_M$ and $(011)_M[0\bar{1}\bar{1}]_M$ are equivalent to the usual b.c.c. slip mode $\{011\}\langle 111\rangle$.

There are no other slip systems which when applied to the WLR theory predict the experimental results and satisfy all the criterions.

The variable V_I has been defined as:

$$V_I = V\delta^3$$

where: V = volume ratio of martensite to austenite

δ = interface dilation parameter

The WLR theory does not recognize the δ but its effect can nevertheless be incorporated in the theory. In the present work the value of V has been assumed to be 1.04 (20) as this is the most common value observed. It was not possible to measure V in the alloys investigated as there is no retained austenite at room temperature.

By varying δ we are effectively introducing a uniform dilation of the habit plane. There is some doubt regarding the validity of the dilation parameter. However it does appear reasonable that the interface between two phases of different volumes will be distorted in some way. Whether it is compressed or expanded one can not say; but the limits of δ are certainly between .986 and 1.015 which correspond to values of V_I of 1.00 and 1.08866 respectively. The physical meaning of the values of δ are as follows: with δ = .986 the "volume" of material at the interface is under

compression so that the volumes of both phases are the same; with $\delta = 1.015$ we have the atomic packing along close packed directions the same in both phases.

The purpose of varying δ in this work was twofold, one to see if the required criterions could be more closely met, and two, to determine if the uncertainty in the true value of V would greatly affect the results. Though calculations were not done for $V_I = 1.05$ it can still be seen from tables 12, 13, and 15 that the calculated data would not vary to any great degree within the range of V_I from 1.03 to 1.05.

It should perhaps be summarized here the evidence which supports the assumption that the crystallography of all six alloys examined can be explained by one treatment.

(1) Previous workers have found the crystallography of low carbon and stainless steels to be the same.

(2) The physical appearance of the surface shears in all six alloys were observed to be the same. The shears in all alloys exhibited at least 5 different orientations.

(3) The appearance of the martensite substructure in all alloys was identical.

(4) At room temperature after quenching no austenite phase is retained.

(5) All the alloys form a b.c.c. martensite.

(6) The martensite traces plotted on a stereogram appear to be consistent with the same crystallographic planes and directions.

CONCLUSIONS

(1) The following alloys were observed to form martensite surface shears:

(1) Pure iron
(2) Fe - .06% C
(3) Fe - .17% C
(4) Fe - 6.0% Mn
(5) Fe - 1.7% Si - 7.83% Mn
(6) Fe - 10.79% Ni

The surface shears suggest an austenite habit plane close to but deviating from $\{111\}$.

(2) A single surface trace analysis of the surface shears in the Fe - 0.17% C and Fe - 6.0% Mn alloys is consistent with the habit plane predicted using the WLR phenomenological martensite theory. This habit plane is 7.12 degrees from $\{111\}_A$.

The observed direction of the martensite crystals in the Fe - 0.17% C and Fe - 6.0% Mn alloys was not found to be consistent with the $\langle 110\rangle_A$ directions. However this does not rule out the possibility that the martensite crystals are plates elongated in a direction close to $\langle 110\rangle_A$ in the habit plane.

(3) The martensite habit plane for all 6 alloys is not a low index plane such as $\{001\}, \{011\}, \{111\}, \{112\}$. The traces were found to be consistent with a $\{145\}$ martensite habit but due to the limitations inherent in a single surface analysis this is not conclusive. TheWLR theory predicts a martensite habit plane 5.03° from $\{145\}$.

The directions parallel to the martensite crystals in all alloys were not found to be consistent with the $\langle 111\rangle$ martensite directions. Hence it can be concluded that the martensite crystals are not needles whose axis is along $\langle 111\rangle_M$ but are rather plates or plates elongated in a given direction within the habit plane.

All evidence suggests that the crystallography in all 6 alloys is the same.

(4) The two inhomogeneous shear systems $(111)_A[\bar{1}\bar{1}2]_A$ and $(100)_A[010]_A$ were found to satisfy all theoretical and experimental criterions when introduced into the WLR theory of martensite transformations. The system $(111)_A[\bar{1}\bar{1}2]_A$ is to be preferred as it generally gives results closer to those desired.

(5) If it is assumed that $V = 1.04$ then it is not necessary to introduce a habit plane dilation parameter δ into the WLR theory to satisfy the experimental results.

SUGGESTIONS FOR FUTURE WORK

There is a vast amount of work still to be done to obtain a complete understanding of the crystallography of iron martensites. Some suggestions relative to the type of martensites examined in this work are:

(1) A thorough study of the following features which characterize the surface shears due to the martensite transformation:

   (a) occurence

   (b) magnitude of shears

   (c) number of orientations formed

(2) Work on ~~determing~~ DETERMINING the austenite habit planes in alloys with no retained austenite but with visible austenite annealing twin vestiges.

(3) More alloys of different compositions from the 6 investigated should be made up and studied to determine the composition range over which the same crystallographic features are observed.

(4) Computer programs should be written so that the effect of variations in certain parameters within the theory can easily be checked as to whether or not they improve the fit between theoretical and experimental results.

APPENDIX I

BAIN DISTORTION AND CORRESPONDENCE MARTICES

A b.c.c. structure can be formed from a f.c.c. structure by a contraction along one f.c.c. axis with a corresponding expansion along the other two axis. This distortion is known as the "Bain Distortion".

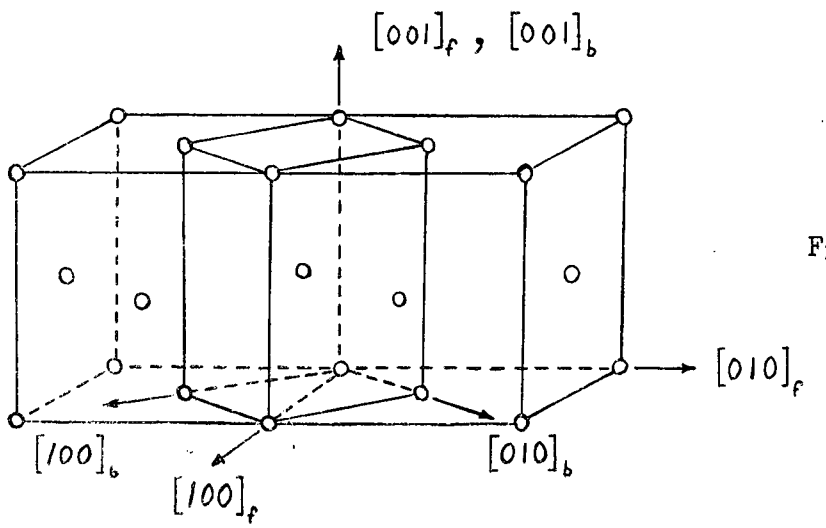

Fig. 28

Shown in Fig. 28 is a b.c.t. cell within the f.c.c. structure; by application of the Bain distortion we transform the b.c.t. cell into a b.c.c. cell.

It can be seen from Fig. 28 that directions in the b.c.c. are related to those in the f.c.c. phase by the equation;

$$\begin{pmatrix} u_1 \\ u_2 \\ u_3 \end{pmatrix}_b = \begin{pmatrix} 1 & \bar{1} & 0 \\ 1 & 1 & 0 \\ 0 & 0 & 1 \end{pmatrix} \begin{pmatrix} u_1 \\ u_2 \\ u_3 \end{pmatrix}_f$$

u_1, u_2, u_3 DIRECTION COMPONENTS

The planes in the two structures are similarly related by:

$$\begin{pmatrix} v_1 \\ v_2 \\ v_3 \end{pmatrix}_b = \begin{pmatrix} 1 & \bar{1} & 0 \\ 1 & 1 & 0 \\ 0 & 0 & 2 \end{pmatrix} \begin{pmatrix} v_1 \\ v_2 \\ v_3 \end{pmatrix}_f$$

v_1, v_2, v_3 NORMAL COMPONENTS

These two matrices are known as the Correspondence Matrices. They are applicable only in the context of Fig. 28; they would not for instance give the b.c.c. martensite habit plane once the f.c.c. austenite habit plane has been found.

THEORETICAL TREATMENT OF MARTENSITE TRANSFORMATION IN STEEL

This appendix will attempt to give a simplified non-rigorous treatment of the theory of martensite transformations following closely the notation and treatment as used by Wayman (3). In this appendix the austenite (f.c.c.) basis and martensite (b.c.c.) basis will be denoted by the subscripts "f" and "b" respectively.

First to define a few of the symbols and terms used:

(1) A matrix will be represented by a capital letter, i.e. A, R .

(2) A vector will be represented by symbols such as $\underline{r}$, $\underline{x}$.

(3) The transpose of a vector or matrix will be identified by priming, i.e. Transpose $A = A'$.

The operation of transposing a matrix simply interchanges rows and columns.

Suppose: $A = \begin{vmatrix} A & B \\ C & D \end{vmatrix}$ then $A' = \begin{vmatrix} A & C \\ B & D \end{vmatrix}$

(4) Vectors will be represented by columns. For example, suppose the vector r has components u, v, w then:

$$\underline{r} = \begin{pmatrix} u \\ v \\ w \end{pmatrix}$$

The transpose of a vector is defined in the same way as matrix. i.e. $\underline{r}' = (u, v, w)$

(5) When the components of a vector are used, these components must be given as the direction cosines.

$$\underline{r}' = |u, v, w| \quad \text{with} \quad u^2 + v^2 + w^2 = 1$$

(6) By a "Change of Basis" we simply mean that we are expressing the components of a vector for instance, relative to a new coordinate system.

This treatment will be based on THE Wechsler, Liebermann, Read (WLR) theory of martensite transformations. This theory makes possible the calculation of the habit plane (in the austenite & martensite) and the shape deformation from a knowledge of the lattice parameters of the f.c.c. and b.c.c. structures and the slip system operative. The fundamental concept underlying the WLR treatment is the existence of a common undistorted plane between the parent (austenite) and product (martensite) structures.

The Bain distortion does not leave a common undistorted plane (the habit plane) between the f.c.c. and b.c.c. structures, and it is therefore necessary to combine with the Bain distortion a critical amount of slip shear. The Bain distortion and slip shear do leave an undistorted plane but they do not leave the plane unrotated, hence a rotation is introduced to return the plane to its original orientation.

The shape deformation (P_1, an invariant plane strain) for the complete transformation can be written as the product of 3 matrices.

$P_1 = RBP$ where: R = the rotation

B = the Bain Distortion

P = the Critical Slip Shear

First the matrix B which represents the Bain distortion will be determined. If the contraction is along $[001]_f$ with equal expansions along $[100]_f$ and $[010]_f$ the b.c.c. structure is obtained; and in this case matrix B has the form:

$$(1) \qquad B = \begin{pmatrix} \eta_1 & 0 & 0 \\ 0 & \eta_1 & 0 \\ 0 & 0 & \eta_3 \end{pmatrix}$$

$$\eta_1 = \left|\sqrt{2}\,\frac{a_b}{a_f}\right|\delta = \left[\sqrt{2}\,\sqrt[3]{\left(\frac{c_b}{a_b}\right)}\right]^{\frac{1}{3}}\delta$$

$$\eta_3 = \left|\frac{c_b}{a_f}\right|\delta = \left[\frac{1}{2}\sqrt[3]{\left(\frac{c_b}{a_b}\right)^2}\right]^{\frac{1}{3}}\delta$$

C_b, a_b are the lattice parameters of the martensite. When the transformation is f.c.c.→b.c.c. $C_b = a_b$. V is the volume ratio of martensite to austenite, about 1.04 for most f.c.c. b.c.c. transformations. The WLR theory considers δ, an interface dilation parameter, to be unity; the factor is used in the Bowles-MacKenzie theory.

Secondly the matrix P which expresses the slip shear must be determined. Let us assume a shear along the unit vector $\underline{a}$ in a plane whose normal is parallel to the unit vector $\underline{v}$; let a 3rd direction be defined by the unit vector $\underline{w}$ given by the cross product. $\underline{w} = \underline{a} \times \underline{v}$

With these 3 new mutually perpendicular unit vectors (orthonormal vectors) a new basis in which the shear has a very single form can be constructed. In other words a basis defined by the directions $\underline{a}, \underline{v}, \underline{w}$, (fig. 29) rather than by the directions $[100]_\varphi$, $[010]_\varphi$, $[001]_\varphi$, has been formed.

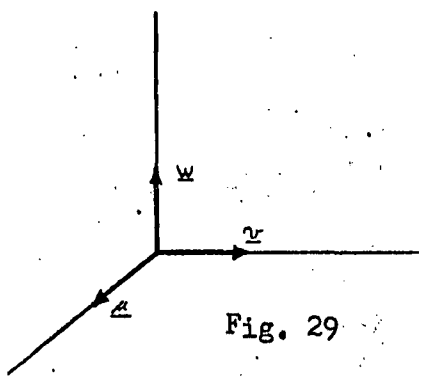

Fig. 29

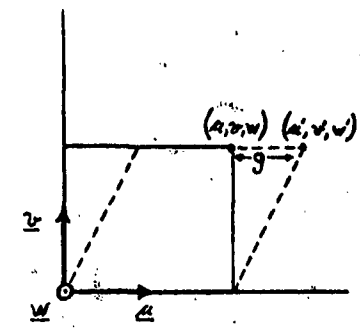

Fig. 30

From Fig. 30:

$$u' = u + gv + 0$$
$$v' = 0 + v + 0$$
$$w' = 0 + 0 + w$$

In Matrix Form

$$\begin{pmatrix} u' \\ v' \\ w' \end{pmatrix} = \begin{pmatrix} 1 & g & 0 \\ 0 & 1 & 0 \\ 0 & 0 & 1 \end{pmatrix} \begin{pmatrix} u \\ v \\ w \end{pmatrix} = P_o \begin{pmatrix} u \\ v \\ w \end{pmatrix}$$

The subscript "o" on the matrix P_o designates the basis. i.e. the new basis is the "o" basis.

Before the product between the two matrices "B" and "P_o" can be

formed the two matrices must be relative to the same basis. Hence the "B" matrix must be referred from the "f" basis (f.c.c. basis) to the "o" basis. This can be done using matrix R_5 (3) whose columns are given by the coordinates of the "o" basis relative to the "f" basis (3). In other words

$$(2) \qquad R_5 = \left(\underline{u}, \underline{v}, \underline{w} \right) = \begin{pmatrix} u_1 & v_1 & w_1 \\ u_2 & v_2 & w_2 \\ u_3 & v_3 & w_3 \end{pmatrix}$$

A "Similarity Transformation" (27, 28) is used to carry out the conversion $B_f \rightarrow B_o$.

$$B_o = R_5' B_f R_5$$

Performing the matrix multiplication using:

$$\underline{u} \cdot \underline{u} = 1 \qquad u \cdot v = 0$$
$$\underline{v} \cdot \underline{v} = 1 \qquad u \cdot w = 0 \qquad \Delta = (\eta_3 - \eta_1)$$
$$\underline{w} \cdot \underline{w} = 1 \qquad v \cdot w = 0$$

$$B_o = \begin{bmatrix} \eta_1 + u_3^2 \Delta & u_3 v_3 \Delta & u_3 w_3 \Delta \\ u_3 v_3 \Delta & \eta_1 + v_3^2 \Delta & v_3 w_3 \Delta \\ u_3 w_3 \Delta & v_3 w_3 \Delta & \eta_1 + w_3^2 \Delta \end{bmatrix}$$

Now B_o P_o can be calculated:

$$(3) \qquad F_o = B_o P_o = \begin{bmatrix} \eta_1 + u_3^2 \Delta & \eta_1 g + u_3 \Delta (u_3 g + v_3) & u_3 w_3 \Delta \\ u_3 v_3 \Delta & \eta_1 + v_3 \Delta (u_3 g + v_3) & v_3 w_3 \Delta \\ u_3 w_3 \Delta & w_3 \Delta (u_3 g + v_3) & \eta_1 + w_3^2 \Delta \end{bmatrix}$$

As the matrix is going to be diagonalized, a symmetric

Matrix J_o is defined as:

$$J_o = F_o' F_o = \begin{bmatrix} \eta_1^2 + u_3^2 (\eta_3^2 - \eta_1^2) & \eta_1^2 g + u_3 \gamma (\eta_3^2 - \eta_1^2) & u_3 w_3 (\eta_3^2 - \eta_1^2) \\ \eta_1^2 g + u_3 \gamma (\eta_3^2 - \eta_1^2) & \eta_1^2 (g^2 + 1) + \gamma^2 (\eta_3^2 - \eta_1^2) & w_3 \gamma (\eta_3^2 - \eta_1^2) \\ u_3 w_3 (\eta_3^2 - \eta_1^2) & w_3 \gamma (\eta_3^2 - \eta_1^2) & \eta_1^2 + w_3^2 (\eta_3^2 - \eta_1^2) \end{bmatrix}$$

where: $\gamma = (u_3 g + v_3)$

The symmetric matrix J_o describes the effect of the Bain distortion and the slip shear g, but the fact that there is a critical value to the shear g has not yet been taken into consideration.

It has been shown (11) that a necessary and sufficient condition for the presence of an undistorted habit plane is for one of the eigenvalues of the distortion matrix J_o to be unity. This condition can perhaps be made plausible by the following consideration. The general form of the eigenvalue equation is:

$$A\,\underline{x} = \lambda\,\underline{x} \qquad \text{where} \qquad A \equiv \text{Matrix}$$

$$\underline{x} \equiv \text{Vector (eigenvector)}$$

$$\lambda \equiv \text{Scalar quantity (eigenvalue)}$$

The equation says that if a matrix A operates upon a vector $\underline{x}$ the length of the vector is changed but not its orientation. Hence if the eigenvalue λ is unity the vector $\underline{x}$ is unrotated and unchanged in magnitude; the conditions desired.

Now forming the equation:

$$J_o\,\underline{x} = \lambda^2\,\underline{x}$$

$$\left(J_o - \lambda^2 \delta_{ij}\right) = 0 \qquad \delta_{ij}$$

For nontrivial solutions of this system of equations the following condition must be met

$$\text{DETERMINANT}\left[J_o - \lambda^2 \delta_{ij}\right] = 0$$

From the determinant the characteristic equation (3) is

$$(\lambda^2)^3 - T(\lambda^2)^2 + Q(\lambda^2) - D = 0$$

$$D = \text{DET}[J_o] = \eta_1^4\,\eta_3^2$$

$$T = \text{TRACE}[J_o] = \eta_1^2\left[2 - 2g\mu_3\upsilon_3 + g^2(1-\mu_3^2)\right] + \eta_3^2\left[1 + 2g\mu_3\upsilon_3 + g^2\mu_3^2\right]$$

$$Q = \eta_1^4\left[1 - 2g\mu_3\upsilon_3 + g^2\upsilon_3^2\right] + \eta_1^2\eta_3^2\left[2 + 2g\mu_3\upsilon_3 + g^2(1-\upsilon_3^2)\right]$$

Three eigenvalues $\lambda_1^2, \lambda_2^2, \lambda_3^2$, are obtained from the characteristic equation. The critical value of shear g is obtained by demanding that one of the eigenvalues (λ_i^2) be unity. Substituting $\lambda_i^2 = 1$, D, T, Q , into the characteristic equation there results the guadratic for the critical shear g.

(4)
$$Ag^2 + Bg + C = 0$$

$$A = (\eta_1^2 - \eta_3^2)(\mu_3^2 + \upsilon_3^2 \eta_1^2) - \eta_1^2(1 - \eta_3^2)$$

$$B = -2(\eta_1^2 - \eta_3^2)(\eta_1^2 - 1)\mu_3 \upsilon_3$$

$$C = (1 - \eta_3^2)(\eta_1^2 - 1)^2$$

In general two different values of g result.

As $(\lambda^2 - 1)$ has been forced to be a factor in the characteristic equation, the other two eigenvalues are obtained by dividing the characteristic equation by $(\lambda^2 - 1)$

To obtain:

(5)
$$(\lambda^2)^2 + (1 - T)(\lambda^2) + D = 0$$

Using one of the values of g in the expression for T, the other two eigenvalues λ_2^2 and λ_3^2 can be solved from equation 5.

Once the eigenvalues λ_1^2, λ_2^2, λ_3^2 are solved for the corresponding eigenvectors $(x^{(1)} y^{(1)} z^{(1)})$ $(x^{(2)} y^{(2)} z^{(2)})$ $(x^{(3)} y^{(3)} z^{(3)})$ can be found as follows:

$$J_o \underline{x} = \lambda^2 \underline{x} \quad \text{or in explicit form} \quad \begin{pmatrix} j_{11} & j_{12} & j_{13} \\ j_{21} & j_{22} & j_{23} \\ j_{31} & j_{32} & j_{33} \end{pmatrix} \begin{pmatrix} x^{(i)} \\ y^{(i)} \\ z^{(i)} \end{pmatrix} = \lambda_i^2 \begin{pmatrix} x^{(i)} \\ y^{(i)} \\ z^{(i)} \end{pmatrix} \qquad i = 1, 2, 3$$

These eigenvectors have been solved for (3, 29)* with the solutions divided

---

* Reference (29) uses differently labeled coordinate system, to use these solutions simply replace the "2" subscripts in ref. (29) with "3".

into 3 cases depending on whether (1) $W_3 = 0$ (2) $W_3 = 1$ (3) $W_3 \neq 0, 1$

The eigenvalues can also be determined by finding a new basis "d" in which the matrix J_o is diagonal in form. These diagonal elements are the eigenvalues λ_1^2, λ_2^2, λ_3^2.

$$J_o = F_o' F_o = R_4 F_d^2 R_4'$$

The matrix R_4 defines the similarity transformation between the "o" basis and the new "d" basis. The columns of R_4 are given by the eigenvectors solved for above. i.e.

$$R_4 = \begin{pmatrix} x^{(1)} & x^{(2)} & x^{(3)} \\ y^{(1)} & y^{(2)} & y^{(3)} \\ z^{(1)} & z^{(2)} & z^{(3)} \end{pmatrix}$$

The basic premise is that in the habit plane any vector $\underline{z}$ must not have its magnitude changed by the action of the matrices B and P. Expressing this algebraically in the "f" basis:

$$\underline{z}' P' B' B P \underline{z} = \underline{z}' \underline{z}$$

The analagous equation in the "d" basis would be

$$\underline{z}' F_d^2 \underline{z} = \underline{z}' \underline{z}$$

which when written in explicit form:

$$\begin{pmatrix} x, y, z \end{pmatrix} \begin{pmatrix} \lambda_1^2 & 0 & 0 \\ 0 & \lambda_2^2 & 0 \\ 0 & 0 & \lambda_3^2 \end{pmatrix} \begin{pmatrix} x \\ y \\ z \end{pmatrix} = \begin{pmatrix} x, y, z \end{pmatrix} \begin{pmatrix} x \\ y \\ z \end{pmatrix}$$

Multiplying out:

$$\left(\lambda_1^2 - 1\right) x^2 + \left(\lambda_2^2 - 1\right) y^2 + \left(\lambda_3^2 - 1\right) z^2 = 0$$

Since λ_1^2 equals unity:

$$\frac{y^2}{z^2} = \frac{1 - \lambda_3^2}{\lambda_2^2 - 1}$$

arbitrarily setting $z = 1$.

into 3 cases depending on whether (1) $W_3 = 0$ (2) $W_3 = 1$ (3) $W_3 \neq 0, 1$

The eigenvalues can also be determined by finding a new basis "d" in which the matrix J_o is diagonal in form. These diagonal elements are the eigenvalues λ_1^2 , λ_2^2 , λ_3^2 .

$$J_o = F_o' F_o = R_4 F_d^2 R_4'$$

The matrix R_4 defines the similarity transformation between the "o" basis and the new "d" basis. The columns of R_4 are given by the eigenvectors solved for above. i.e.

$$R_4 = \begin{pmatrix} x^{(1)} & x^{(2)} & x^{(3)} \\ y^{(1)} & y^{(2)} & y^{(3)} \\ z^{(1)} & z^{(2)} & z^{(3)} \end{pmatrix}$$

The basic premise is that in the habit plane any vector $\underline{z}$ must not have its magnitude changed by the action of the matrices B and P. Expressing this algebraically in the "f" basis:

$$\underline{z}' P' B' B P \underline{z} = \underline{z}' \underline{z}$$

The analagous equation in the "d" basis would be

$$\underline{z}' F_d^2 \underline{z} = \underline{z}' \underline{z}$$

which when written in explicit form:

$$\begin{pmatrix} x, y, z \end{pmatrix} \begin{pmatrix} \lambda_1^2 & 0 & 0 \\ 0 & \lambda_2^2 & 0 \\ 0 & 0 & \lambda_3^2 \end{pmatrix} \begin{pmatrix} x \\ y \\ z \end{pmatrix} = \begin{pmatrix} x, y, z \end{pmatrix} \begin{pmatrix} x \\ y \\ z \end{pmatrix}$$

Multiplying out:

$$\left(\lambda_1^2 - 1\right) x^2 + \left(\lambda_2^2 - 1\right) y^2 + \left(\lambda_3^2 - 1\right) z^2 = 0$$

Since λ_1^2 equals unity:

$$\frac{y^2}{z^2} = \frac{1 - \lambda_3^2}{\lambda_2^2 - 1}$$

arbitrarily setting $z = 1$.

(6) $$y = \pm\left(\frac{1-\lambda_3^2}{\lambda_2^2-1}\right)^{\frac{1}{2}} = \delta_K K \qquad \text{Where} \qquad \delta_K = \pm 1$$

Hence one undistorted vector in the habit plane is $[0, \delta_K K, 1]$; another as can be seen by inspection is $[1,0,0]$. The normal to the habit plane p_1 is then given by the cross product:

$$[1,0,0] \times [0, \delta_K K, 1] = [0, 1, \delta_K K]$$

Normalizing

(7) $$p_{1(d)} = \frac{1}{(1+K^2)^{\frac{1}{2}}}[0, 1, \delta_K K]$$

There are in general 4 solutions to $p_{1(d)}$, corresponding to the 2 values of g and δ_K. The degeneracy of solutions is discussed by Wechsler (29). $p_{1(d)}$ is a unit vector along the habit plane normal relative to the "d" basis.

The eigenvectors which comprise R_4 can be referred to the "f" basis from the "o" basis by the matrix R_5:

(8) $$\begin{pmatrix} x^{(i)} \\ y^{(i)} \\ z^{(i)} \end{pmatrix}_f = \begin{pmatrix} u_1 & v_1 & w_1 \\ u_2 & v_2 & w_2 \\ u_3 & v_3 & w_3 \end{pmatrix} \begin{pmatrix} x^{(i)} \\ y^{(i)} \\ z^{(i)} \end{pmatrix}_o \qquad i = 1, 2, 3$$

The $[x^{(i)}, y^{(i)}, z^{(i)}]_f$ form the columns of the matrix which expresses the transformation between the "d" basis and the "f" basis. Hence the habit plane relative to the "f" basis is found from:

(9) $$p_{1(f)} = \begin{pmatrix} x^{(1)} & x^{(2)} & x^{(3)} \\ y^{(1)} & y^{(2)} & y^{(3)} \\ z^{(1)} & z^{(2)} & z^{(3)} \end{pmatrix}_f p_{1(d)}$$

$p_{1(f)}$ is a unit vector parallel to the habit plane normal relative to the austenite axis.

Next must be found the habit plane relative to the martensite axis. The directions $[1\bar{1}0]_f$, $[110]_f$, $[001]_f$ are not rotated by the Bain distortion.

as can be seen by the application of the matrix B to these three directions. Furthermore the lattice invariant shear P has no effect on crystallographic directions. Hence in the expression for the complete martensite transformation $P_1 = RBP$, only the rotation R can affect the crystallographic directions. The martensite habit plane is given as the direction cosines of the habit plane measured from the martensite axis. The martensite axes (fig. 28) are given by the effect of the rotation R on the three austenite directions.

The matrix R can be determined by realizing that it must counteract the rotation introduced by BP. If F_f is applied to any two vectors in the austenite habit plane, by the use of Euler's theorem (3) the angle of rotation and rotation axes necessary to return these two vectors into their initial positions can be determined. As so far only F_o has been determined, F_f can by obtained by carrying out a transformation from the "o" to the "f" basis. This is done from the equation:

(10) $$F_f = R_S F_o R_S'$$

Suppose that ν and σ are any two vectors in the austenite habit plane, then applying F_f:

(11) $$\nu_1 = F_f \nu \qquad \sigma_1 = F_f \sigma$$

then by Euler's theorem a vector along the desired axis of rotation is

(12) $$\frac{[\nu_1 - \nu] \times [\sigma_1 - \sigma]}{[\sigma_1 - \sigma] \cdot [\nu_1 + \nu]} = \underline{r}$$

The magnitude of this vector determines the angle of rotation θ.

(13) $$|\underline{r}| = \mathrm{TAN}\left(\frac{\theta}{2}\right)$$

The desired unit vector with components P_1, P_2, P_3 is obtained by normalizing $\underline{r}$.

The general form of the matrix which expresses a rotation by an angle θ about the unit direction $[P_1, P_2, P_3]$ can be shown to be (3)

(14) $$R = \begin{bmatrix} P_1^2(1-\cos\theta) + \cos\theta & P_1P_2(1-\cos\theta) - P_3\sin\theta & P_1P_3(1-\cos\theta) + P_2\sin\theta \\ P_2P_1(1-\cos\theta) + P_3\sin\theta & P_2^2(1-\cos\theta) + \cos\theta & P_2P_3(1-\cos\theta) - P_1\sin\theta \\ P_3P_1(1-\cos\theta) - P_2\sin\theta & P_3P_2(1-\cos\theta) + P_1\sin\theta & P_3^2(1-\cos\theta) + \cos\theta \end{bmatrix}$$

Now as previously mentioned the position of the martensite axes relative to the austenite axes after the application of P_1 are given by:

(15) $\quad R[1\bar{1}0] = [a, b, c] \qquad R[110] = [d, e, f] \qquad R[001] = [g, h, i]$

These components form the matrix which expresses the transformation between the austenite and martensite basis. Hence the unit vector parallel to the martensite habit plane $P_{1(b)}$ is obtained from the equation:

(16) $$P_{1(b)} = \begin{pmatrix} a & b & c \\ d & e & f \\ g & h & i \end{pmatrix} P_{1(f)} = A' P_{1(f)}$$

The shape deformation relative to the austenite axes is given by

(17) $$P_1 = R B P = R F_f$$

applying $R F_f$ to the habit plane normal in the parent material (austenite):

$$R F_f P_{1(f)}$$

The direction of the shape deformation is then given by vector subtraction

$$R F_f P_{1(f)} - P_{1(f)}$$

The magnitude of the vector $R F_f P_{1(f)} - P_{1(f)}$ gives the magnitude of the shape deformation.

Now to consider the parallelism between directions and planes in the austenite and martensite. For example, suppose it is desired to calculate the angle θ between $[111]_f$ and $[011]_b$:

(1) Form $A'[111]_f$ and normalize.

(2) Take dot product with $[011]_b$.

(3) Divide by $\sqrt{2}$ to obtain $\cos\theta$.

NUMERICAL CALCULATIONS

The following is a suggested procedure for calculating numerically the austenite and martensite habit planes and the shape deformation.

(1) Assume a specific slip system of the form $(\mu_1, \mu_2, \mu_3)[\upsilon_1, \upsilon_2, \upsilon_3]$

(2) Calculate η_1 and η_3 equation 1.

(3) Solve for the two values of g, equation 4.

(4) Pick one value for g (usually the smaller) and solve for λ_2^2 and λ_3^2, equation 5.

(5) Calculate the habit plane normal relative to the "d" basis, equation 7.

(6) Depending on the value of ω_3 calculate the three eigenvectors relative to the "d" basis. References (3, 29). See text of appendix.

(7) Refer these eigenvectors to the "f" basis, equation 8.

(8) Calculate the habit plane normal in the "f" (austenite) basis, equation 9.

(9) Calculate F_o, equation 3.

(10) Calculate F_f, equation 10.

(11) Choose any two vectors ν, σ in the austenite habit plane, work out equation 11.

(12) Calculate $\underline{r}$, equation 12. Normalize $\underline{r}$.

(13) Calculate θ equation 13.

(14) Calculate R, equation 14.

(15) Work out equation 15.

(16) Obtain the martensite habit plane from equation 16.

(17) The shape deformation is determined as given from equation 17 onwards.

APPENDIX II

INVESTIGATION OF MARAGING PROPERTIES OF Fe-Mn-Si SYSTEM

GENERAL

The term "maraging" is used to describe an age hardening treatment given to a carbon free iron martensite structure. There are three basic types of iron-nickel base maraging steels; those containing 12% Ni (32), 18% Ni (31, 33, 34, 35, 36), 20 - 25% Ni (36). The high nickel content is to ensure a ductile martensite structure while supplementary additions such as molybdenum, cobalt, titanium are added to cause the age hardening response.

The most useful maraging steel to date has proven to be that with the approximate composition Fe-18% Ni-8% Co-4% Mo-0.4% Ti. The typical aging treatment for this steel simply consists of a one hour anneal at 800 degrees C, an air cool to room temperature followed by a three hour aging treatment at 450° C . The strengthening appears to result from ordering and precipitation reactions, but the exact mechanism's are not clearly understood and are the subject of much investigation.

The great similarity between the iron-nickel and iron-manganese binary phase diagrams (Fig. 32) suggests that it might be possible to develop a manganese maraging steel in analogy to the nickel maraging steels (31→36). A partial substitution of manganese for nickel has already been affected by Patterson and Richardson (37) in that they developed a steel of composition 12.5% Ni, 2% Mn, 8% Co, 4% Mo, 0.2% Ti, 0.1% Al which is comparable with the usual Fe-Ni maraging steels. They found that manganese substitutes equivalently for nickel in a ratio of one part Mn for 3 parts Ni. They also suggest that to improve the Fe-Ni-Mn maraging steels an increase in Mn along with a corresponding drop in cobalt should be investigated. Goldman and Manec (38) have carried out experiments on the kinetics and mechanism of hardening in a

Fe-12% Mn-5% Ni-4% Ti maraging steel, while Keiichi Ohta (39) reports that in a Fe-4.85% Ni-2.66% Mn-2.52% Si-0.52% Ti steel there is an increase in hardness from 28 to 53 Rockwell C on tempering 4 hours at 500° C. Earlier work by Decker, Eash and Goldman (31) had suggested that manganese had undesirable effects but this now appears to be erroneous, at least up to the additions reported above. Also Kattus (40) has developed a 3-11% Mn, 1.5 - 2.0% Si, 0.6 - 1.2% Ti, 0.4 - 3.4% Mo steel which shows an ultimate strength increase from 85,000 to 160,000 psi after aging for several hours at 480° C. Richardson (41) discovered that Fe-Mn-Ni alloys without auxiliary hardeners shows the typical increase in strength after a maraging treatment.

The aim of the present investigation was to develop a nickel free maraging steel with the use of manganese and silicon additions. Maraging properties were to be looked for among those alloys which had a soft martensite structure on cooling from the austenite. The manganese was added to ensure a martensitic transformation while the silicon addition was to provide the hardening mechanism. As can be seen from the Fe-Si binary phase diagram (Fig. 33), Fe-Si alloys in the region of 6% can take part in an ordering reaction. The idea was to quench the alloys from the disordered phase (α) so that they would still be disordered, and hopefully, soft at room temperature. Then with the subsequent aging treatment within the ordered α' phase it was hoped that the alloys would harden. The maraging properties of the Fe-Mn binary were also examined.

In order to determine the optimum alloy composition the manganese content was varied from 0 to 20% with variations of silicon between 0 and 6%. The effect of varying the aging temperature was also investigated.

ALLOY PREPARATION AND ANALYSIS

The materials and the procedure used in the preparation of the alloys are as given in "Experimental" of this thesis. A total of 17 alloys were cast but five had to be discarded because the composition was not homogeneous.

The methods of alloy analysis are the same as those used in the "Experimental". It was not found possible to analyse for silicon by X-ray fluorescence; hence the Si content was assumed to be correct whenever the Mn content was analysed to be so. The analysis of the alloys used is given in Table 16.

Details of preparation of specific alloys are shown on the age hardening curves Figs. 34 to 42. Homogenization was carried out in a horizontal tube furnace under an atmosphere of dissociated ammonia ($3H_2 + N_2$).

Specimans were quenched directly from a vertical tube furnace into brine or water. Specimans were polished before hardness tests, hence any effects due to the dissociated ammonia atmosphere should be minimized.

The aging curves were obtained by holding the speciman at temperature for a given length of time, quenching in water, measuring the hardness and then returning the same speciman to the furnace for another predetermined length of time before repeating the process. No special atmosphere was used for the aging tests.

If there is a martensite transformation present in a speciman the cooling curve should show a decrease in slope at the transformation temperature. A Chromel - Alumel thermocouple was spot welded to the sample which was then heated into the austenite region with a torch. The thermocouple was attached to an oscilloscope which displayed the cooling curve as a function of millivolts and time. The formation of bubbles on the surface of the speciman when quenching in water prevents a smooth cooling curve and hence covers any change

in slope. It was therefore necessary to coat the surface of the speciman on the side of the thermocouple with refractory cement. While this procedure reduces slightly the cooling rate it does allow a smooth cooling curve to be obtained.

Specimans for optical examination were lapped progressively down to 3/0 grit paper, then polished with diamond paste. Polishing with alumina was found to cause pitting. Etching was performed with a 1% solution of HNO_3 in alcohol (Nital).

Specimans used on the diffractometer were approximately $\frac{3}{4}$" x $\frac{3}{4}$" x $\frac{1}{4}$" with one face polished with 3/0 grit paper.

RESULTS

The two alloys Fe - 6.0% Mn and Fe - 1.7% Si - 7.83% Mn were found to exhibit surface shears (Figs. 9 and 11) which are the commonly accepted criterion as to whether or not a martensitic transformation has taken place. No other alloys were examined for surface shears. These two alloys and the four given below did have the same etched structure (Fig. 31):

Fe - 7.3% Mn
Fe - 9.5% Mn
Fe - 1.0% Si - 4.5% Mn
Fe - 4.0% Si - 8.0% Mn

The structure in Fig. 31 is very similar to that found in Fe-Ni martensites by Owen et. al. (13). None of the alloys given in Table 16 other than the above six were found to show this martensitic etched structure.

Fig. 31: Typical Massive Martensite Structure. 175 X. Surface Polished and Etched in Nital.

The identifiable phases as determined from the studies on the diffractometer are given in Table 17.

Cooling curves of the following alloys were studied: Fe - 7.3% Mn, Fe - 4.79% Si - 8.08% Mn, Fe - 5.15% Si - 9.43% Mn, Fe - 5.93% Si - 13.58% Mn, Fe - 6.30% Si - 19.40% Mn. The expected cooling curve arrest during air cooling and water quenching was only observed with the Fe - 7.3% Mn alloy.

Age hardening experiments were carried out on all alloys (Table 16) except Fe - 7.3% Mn, Fe - 9.5% Mn and Fe - 16.5% Mn. See Figs. 34 to 42 for the age hardening curves obtained.

		METHOD OF ANALYSIS	
	ALLOY	CHEMICAL	X-RAY FLUORESCENCE
1	Fe-6.0% Mn		X
2	Fe-7.3% Mn	X	
3	Fe-9.5% Mn		X
4	Fe-16.5% Mn		X
5	Fe-1.0% Si-4.5% Mn		X
6	Fe-1.7% Si-7.83% Mn	X	
7	Fe-4.0% Si-8.00% Mn	X	
8	Fe-4.79% Si-8.08% Mn		X
9	Fe-4.79% Si-9.43% Mn	X	
10	Fe-5.93% Si-13.58% Mn	X	
11	Fe-6.30% Si-19.40% Mn	X	
12	Fe-2.50% Si-6.0% Mn-.5 Ti		X

Table 16. Analysis of Alloys in Weight Percent.

ALLOY	COOLING MEDIA					OBSERVED STRUCTURE		
	FURNACE	AIR	WATER	BRINE	LIQ. N_2	α (b.c.c.)	γ (f.c.c.)	ϵ (h.c.p.)
1. Fe-6.0Mn		X				X		
2. Fe-7.3Mn		X				X		
3. Fe-9.5Mn		X				X		
4. Fe-16.5Mn		X				?	X	X
					X		X	X
5. Fe-1 Si-4.5 Mn		X				X		
6. Fe-.17 Si-7.83 Mn	X					X		
				X		X		
7. Fe-4.0 Si-8.0 Mn	X					X		
				X		X		
8. Fe-4.79 Si-8.08 Mn		X				X		
			X			X		
9. Fe-5.15 Si-9.43 Mn		X				X		
			X			X		
10. Fe-5.93 Si-13.58 Mn			X			X	X	X
11. Fe-6.30 Si-19.40 Mn		X				?	X	X
			X			X		
12. Fe-2.5 Si-6.0 Mn-0.5 Ti		X				X		

Table 17. Structures Present After Cooling from the Austenite Region.

DISCUSSION OF RESULTS

OPTICAL AND DIFFRACTOMETER STUDIES

Of the four Fe-Mn binary alloys studied the Fe-6.0% Mn, Fe-7.3% Mn and Fe-9.5% Mn had the typical massive martensite appearance (Fig. 30) while the Fe-16.5% Mn did not. Further as can be seen from Table 17 the first 3 alloys form a b.c.c. iron phase, whereas the Fe-16.5% Mn has a partial f.c.c., partial h.c.p. structure with the presence of the b.c.c. phase questionable. These results are in agreement with Troiano and McGuire (42). The appearance of the ϵ -phase in the Fe-Mn binary complicates the situation and it is not possible to form a completely analagous range of alloys to those found in iron-nickel up to 33 wt. % (8). An alloy which forms the h.c.p. ϵ - phase in a similar manner is Fe-18% Cr - 9% Ni. Otte (43) has associated the presence of stacking faults in the 18-9 stainless steel with the formation of the ϵ - phase. The fact that susceptibility to faulting increases with Mn but is little affected by Ni content leads one to suspect that the formation of the ϵ - phase in the Fe-Mn binary but its absence in the Fe-Ni binary is attributable to faulting.

It is commonly recognized in the literature (42, 43, 45 , 46) that the ϵ -phase is intermediate in the transition from f.c.c. to b.c.c. structures. As can be seen from Table 17 the alloy Fe-6.30% Si-19.40%Mn forms γ and ϵ structures on an air cool but on the more rapid water quench it forms an α structure. Also an air cooled sample of Fe-16.5% Mn was cold worked with the result that the ϵ and α phases formed. Hence in effect the following transformations were observed.

$\gamma \rightarrow \gamma + \epsilon$	Fe-6.30% Si-19.40%Mn	Air Cool
$\gamma \rightarrow \alpha$	Fe-6.30% Si-19.40% Mn	Water Quenched
$\gamma \rightarrow \gamma + \epsilon \rightarrow \epsilon + \alpha$	Fe-16.5% Mn	Cold Work

These three equations strongly suggest that ϵ is an intermediate phase between the γ and ϵ structures.

The ternary alloys studied which displayed the massive martensite structure (Fig. 31) were Fe - 1.0% Si - 4.5% Mn, Fe - 1.7% Si - 7.83% Mn and Fe - 4.0% Si - 8.0% Mn. The Fe - 1.7% Si - 7.83% Mn alloy exhibited martensitic surface shears; it is probable that the other two ternary alloys would have also if they had been studied. From Table 17 it can be seen that these 3 alloys all possess an α structure on air cooling to room temperature. However this fact is not necessarily consistent with these 3 alloys being martensitic because most of the other alloys also have an α structure on air cooling. The explanation probably lies in the silicon content. As can be seen from the Fe-Si phase diagram (Fig. 33) there is a γ loop up to about 2.5wt% Si, and as the Fe-Mn binary is γ at sufficiently high temperatures a $\gamma \rightarrow \alpha$ transformation is obtained on quenching Fe-Mn-Si (Si $<$ 2.5Wt.%) systems. At silicon contents slightly over 2.5% the influence of the γ Fe-Mn structure will predominate and the $\gamma \rightarrow \alpha$ transformation still forms; which accounts for the Fe-4.0% Si - 8.0% Mn system being martensitic. Also this alloy was not analysed for silicon loses on casting and hence its true silicon content is likely somewhere between 3.5 and 4.0%. As the Fe - 4.79% Si - 8.08% Mn alloy is reached the martensitic structure no longer forms on cooling and it appears that now the influence of the silicon predominates and the equilibrium structure is preserved from high to room temperature. This reasoning also holds for the Fe - 5.15% Si - 9.43% Mn alloy. In the two alloys of higher manganese content predominance may be returning to the Mn as we observe (Fig. 5) the γ structure in both the Fe - 5.93% Si - 13.58% Mn and Fe - 6.30% Si - 19.40%Mn. In the alloy of lower Mn content (Fe - 5.93% Si - 13.58% Mn) there is some question as to whether or not the observed α is the product of a martensitic transformation; but in the alloy of higher Mn content the fact that the α only forms on rapid quenching suggests that it is martensitic. To confirm

this it would be necessary to determine whether or not shears form on the surface of a speciman which had been polished before quenching from high temperatures.

No optical or cooling curve studies were made on the Fe-2.5% Si-6.0%Mn 0.5% Ti alloy but in analogy to alloys of similar Mn and Si contents it is probably safe to assume that the α structure formed at room temperature is martensitic.

COOLING CURVES:

Of those alloys tested only the Fe - 7.3% Mn showed a change in slope in its cooling curve. Because of the experimental limitations it is not possible to determine the transition temperature with any more accuracy then to say that it lies somewhere between 360 and 390° C. This temperature range was observed with both air cooled and water quenched specimans. Gomersall and Parr (44) carried out cooling curve experiments in the same way and obtained comparable results. As no cooling curve arrest was noticed when water quenching the Fe - 6.30% Si - 19.40% Mn alloy it would appear not to be martensitic; the optical studies also bear this out. However the fact that its water quenched structure suggests a martensitic transformation shows that more work must be done on this alloy.

AGING TESTS:

The data obtained is presented graphically in Figs. 34 to 42. All of the alloys except Fe - 4.79% Si - 8.08% Mn showed a tendency to harden. The greatest hardness increase was only 8 Rockwell C points (Fe - 5.93% Si - 13.58% Mn) while the average was 2 $\rightarrow$ 3 Rc Points. Kattus (40) has developed alloys similar in composition to those examined here which show a hardness increment of some 25 points (Rc 10 to Rc 35). Two of the alloys, Fe - 4.0% Si-8.0% Mn and Fe - 4.79% Si - 8.08% Mn do have this hardness but it was not found

possible to obtain them in the soft condition before the maraging treatment.

The 4 alloys most extensively studied, Fe - 6.0% Mn, Fe - 1.0% Si - 4.5% Mn, Fe - 1.70% Si - 7.83% Mn, and Fe - 4.0% Si - 8.0% Mn do show a typical type of maraging curve. The optimum aging temperature and aging time for the highest strength was 450° C. and approximately 1/2 hour for all 4 alloys. With aging at 400, 500, and 600° C the same strength was not reached. Aging at 400° C does not cause the curves to fall off appreciably after 4 hours as they do with aging at 500 and 600° C. The fall off in hardness with high temperature aging is probably due to a breakdown of the martensite structure with a reversion to the austenite. All 4 of these alloys are martensitic after quenching from the austenite. The other alloy which was martensitic at room temperature was Fe - 2.5% Si - 6.0% Mn - 0.5% Ti, and while it was not as extensively studied as the above four it did show similar maraging curves.

The other 4 alloys whose aging characteristics were investigated are Fe - 4.79% Si - 8.08% Mn, Fe - 5.15 % Si - 9.43% Mn, Fe - 5.93% Si - 13.58%Mn, and Fe - 6.30% Si - 19.40%Mn. These alloys are probably not martensitic at room temperature with the possible exception of Fe - 6.30% Si - 19.40% Mn in the water quenched condition. The above non-martensitic alloys lose their hardness much more slowly while aging at 600° C than do the 5 martensitic alloys. This may be expected as the softening mechanism operable in the martensitic alloys will not apply here, where the softening is likely due to a realignment and annealing out of dislocations.

The slight hardening increment observed for all alloys except Fe - 4.79% Si - 8.08% Mn, is probably due to an ordering process involving the silicon. According to the Fe-Si phase diagram (Fig. 33) the ordering should not take place until 6% Si at 450° C. The fact that the two alloys which show the largest hardening increment also contain the largest silicon content support

the fact that silicon is taking part in ordering. Other work conducted within the department on the Fe-Si binary is consistent with the idea that ordering causes slight hardening.

FUTURE WORK

Much work remains to be done on these Fe-Mn base maraging steels in an attempt to obtain a useful product. Possible suggestions are as follows:

1. Continue the systematic investigation of the maraging properties by varying (a) proportions of manganese and silicon (b) aging temperatures and time.
2. Examine the ordering reaction in the Fe-Si binary in an attempt to determine if the silicon addition is beneficial.
3. Attempt to explain why the Fe-Mn binary with no silicon additions also shows a hardening increment.
4. Study effects of additional elements such as titanium.
5. Study the occurence and crystallography of the h.c.p. ϵ phase in the Fe-Mn binary.

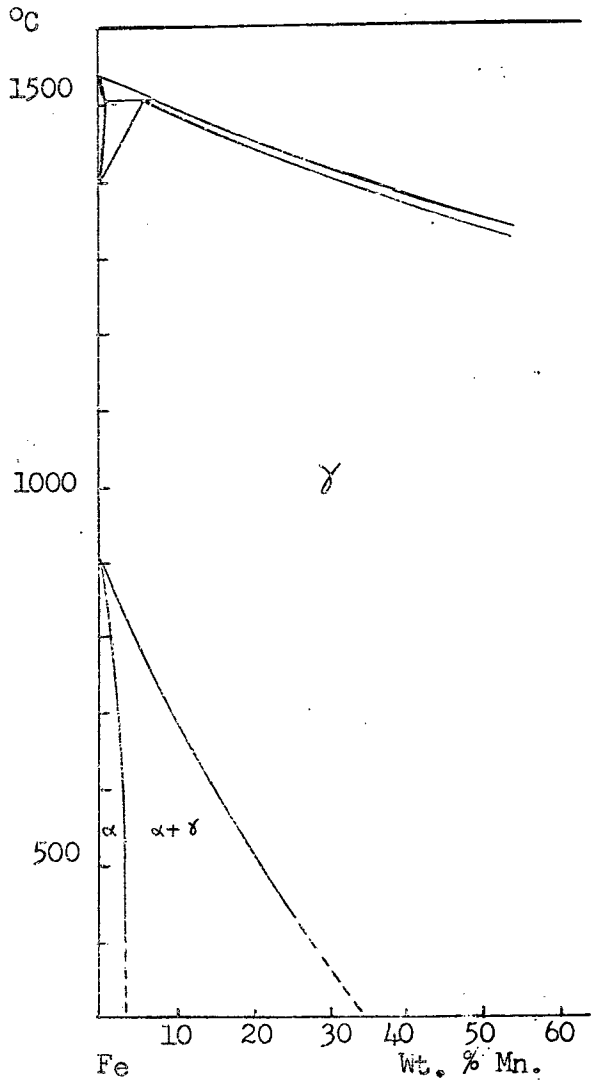

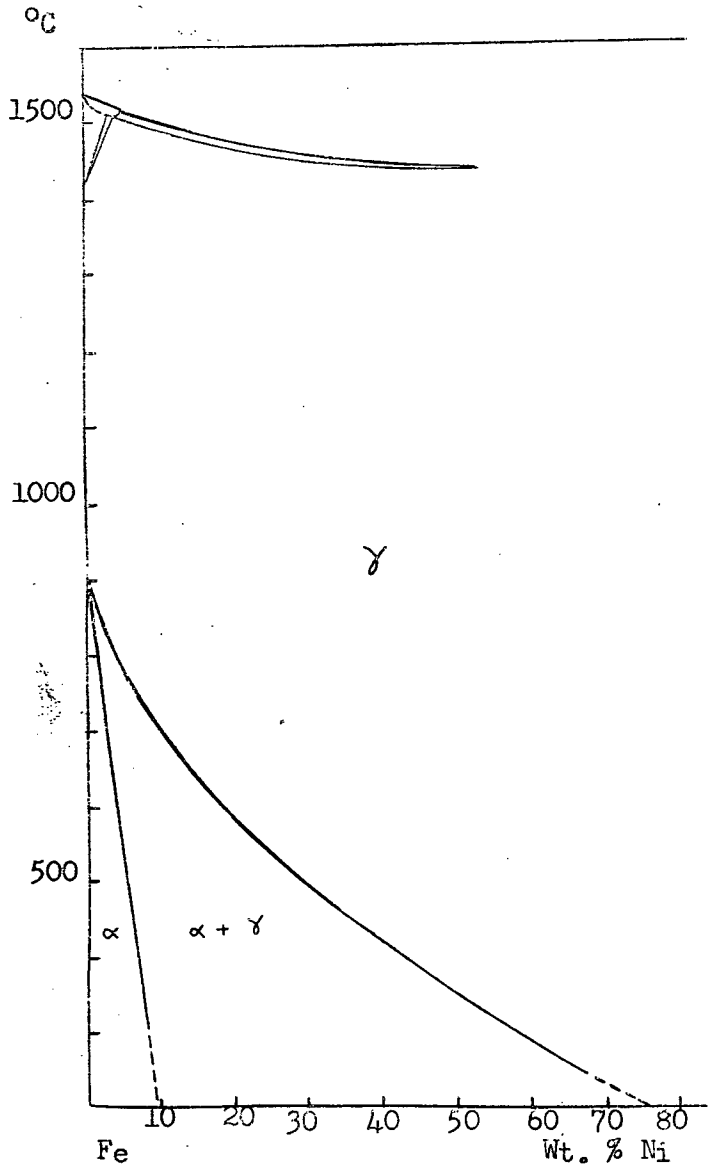

Fig. 32: Fe - Mn and Fe - Ni Binary Phase Diagrams

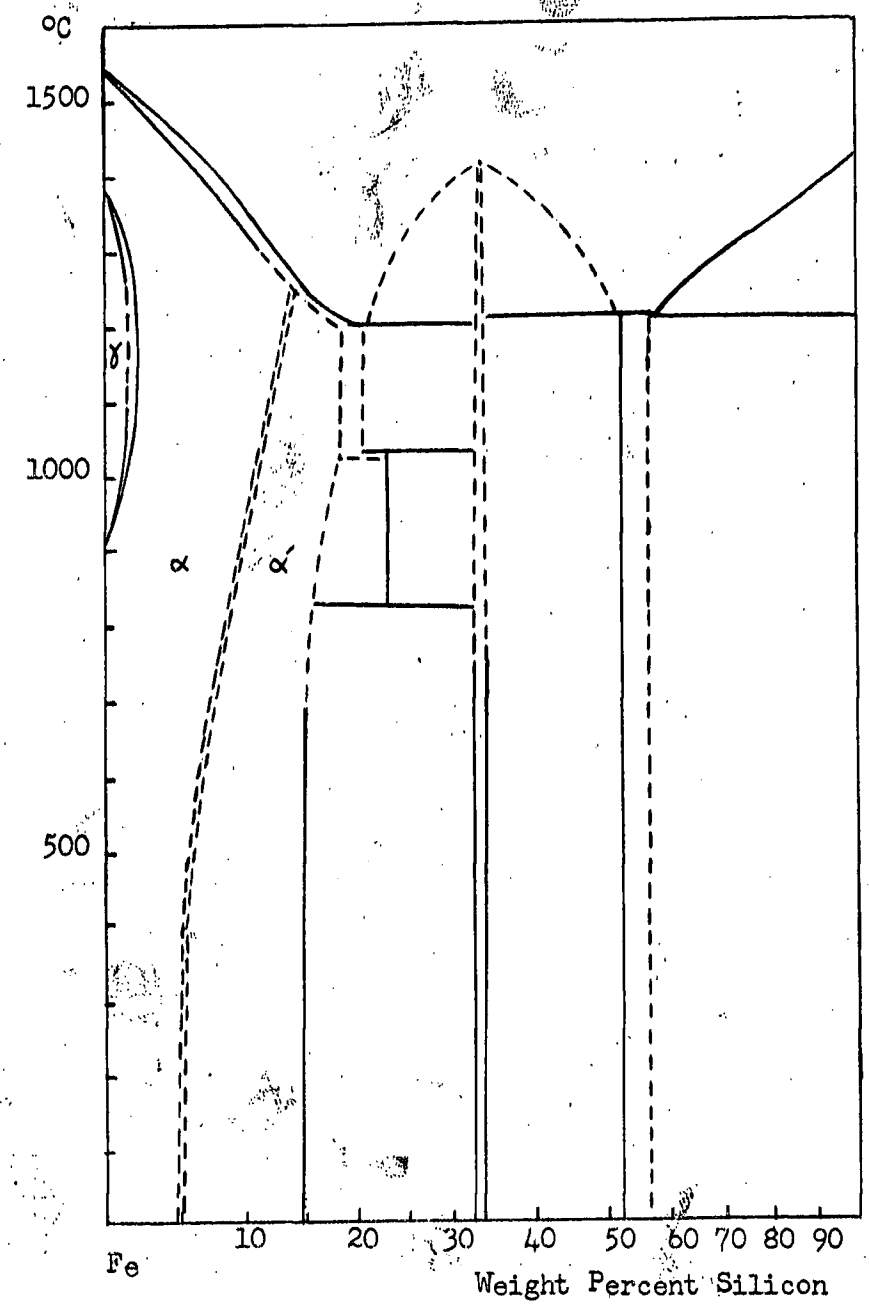

Fig. 33: Fe - Si Binary Phase Diagram.

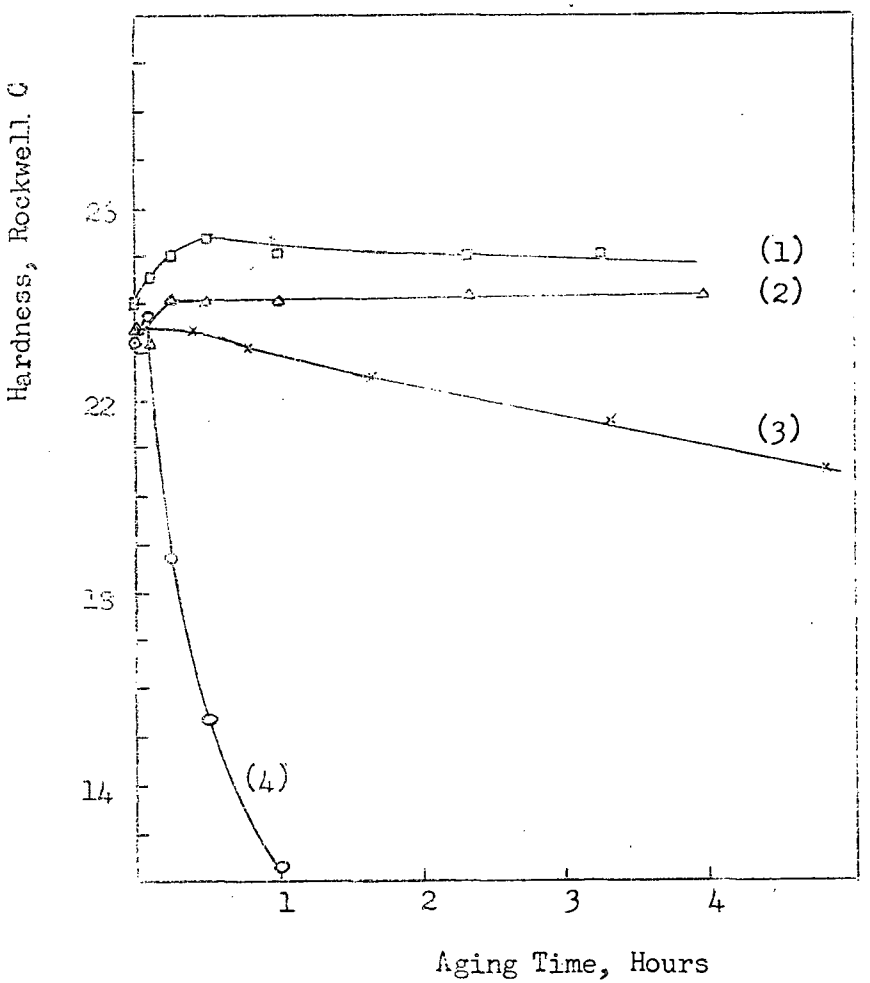

Fig. 34. Fe - 1.0% Si - 4.5% Mn. Aging curves.
- Hotrolled 950° C.
- Annealed 950° C, 1/2 hour, air cooled.
- Curve (1) Aged 450° C
  Curve (2) Aged 400° C
  Curve (3) Aged 500° C
  Curve (4) Aged 600° C

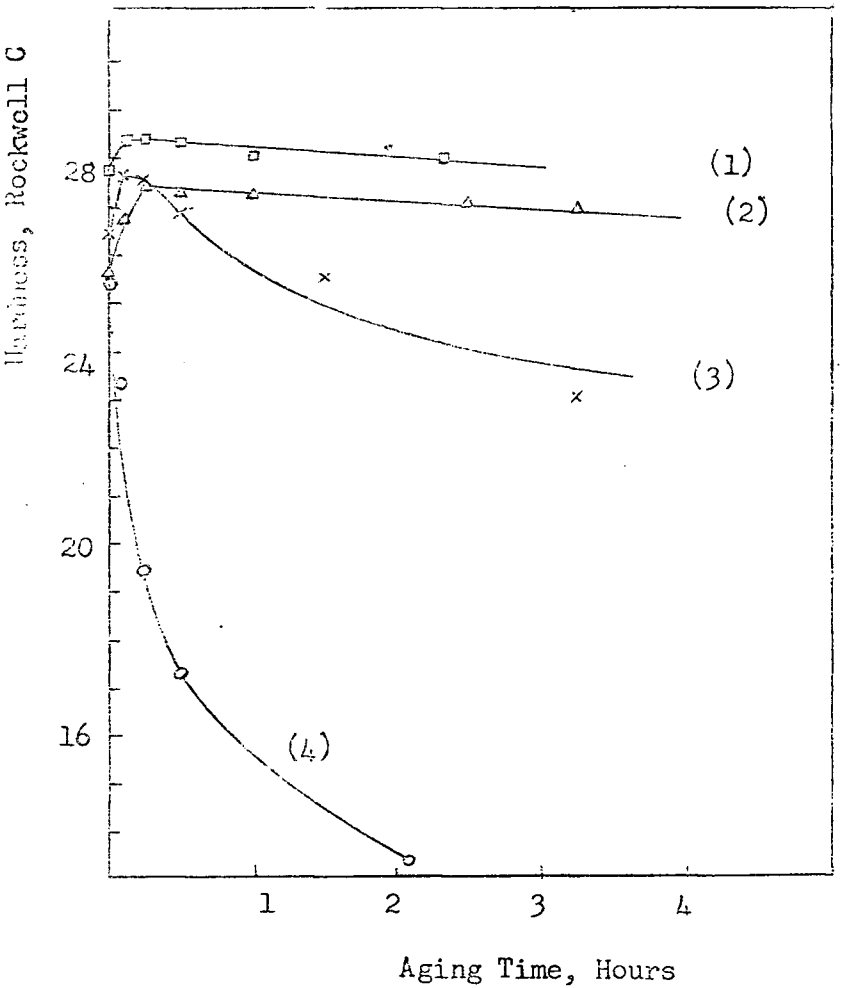

Fig. 35. Fe - 6.0% Mn. Aging curves.
- Hotrolled 950° C
- Annealed 950° C, 1/2 hour, air cooled
- Curve (1) Aged 450° C
  Curve (2) Aged 400° C
  Curve (3) Aged 500° C
  Curve (4) Aged 600° C

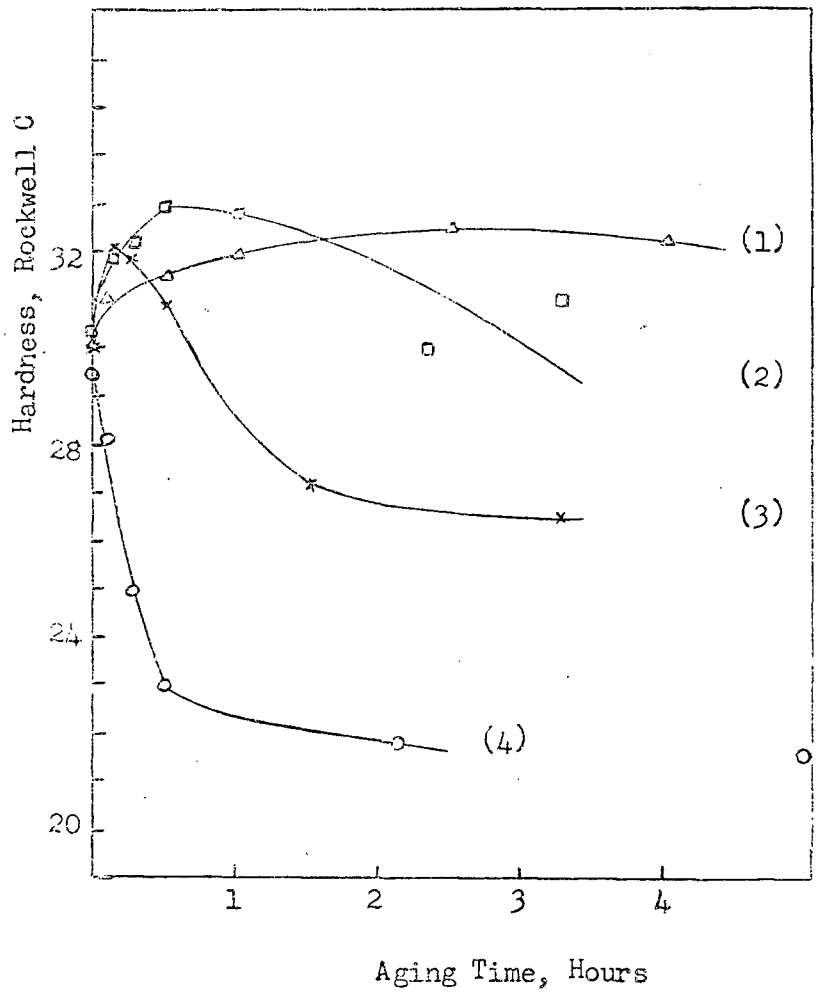

Fig. 36. Fe - 1.70% Si - 7.83% Mn. Aging Curves
- Hotrolled 950° C.
- Annealed 950° C, 1/2 Hour, Air Cooled.
- Curve (1) Aged 400° C.
  Curve (2) Aged 450° C.
  Curve (3) Aged 500° C.
  Curve (4) Aged 600° C.

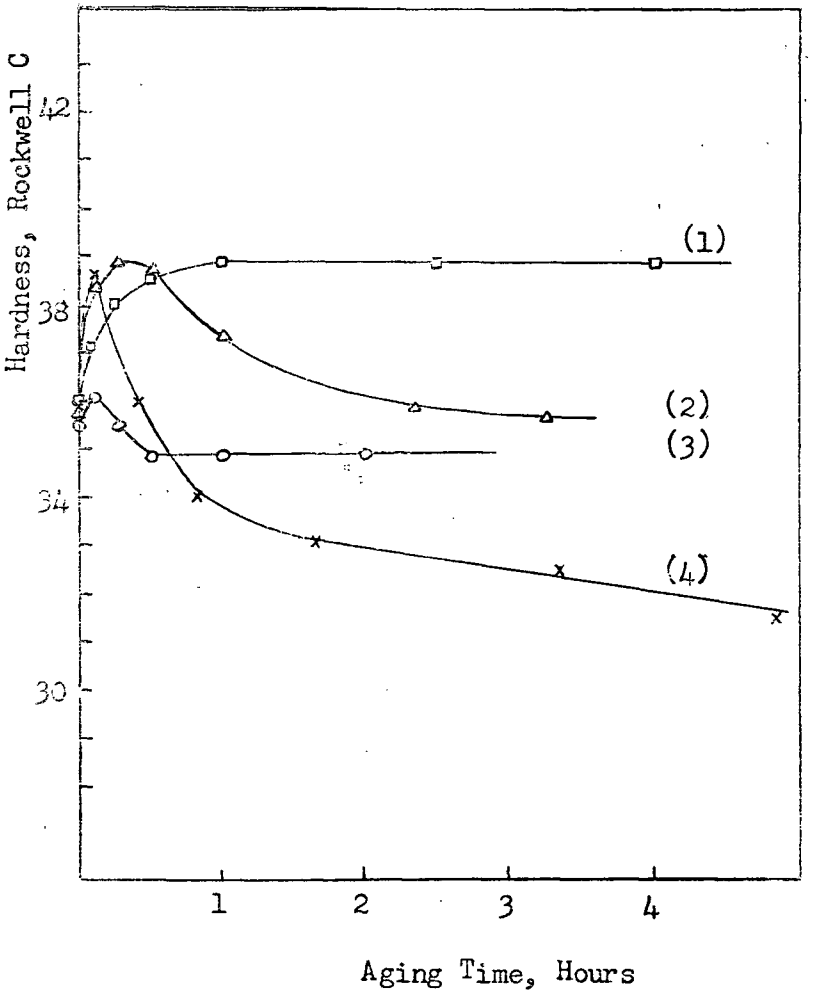

Fig. 37. Fe - 4.0% Si - 8.0% Mn, Aging Curves.
-Hotrolled 950° C.
-Annealed 950° C, 1/2 Hour, Air Cooled.
-Curve (1) Aged 400° C.
Curve (2) Aged 450° C.
Curve (3) Aged 600° C.
Curve (4) Aged 500° C.

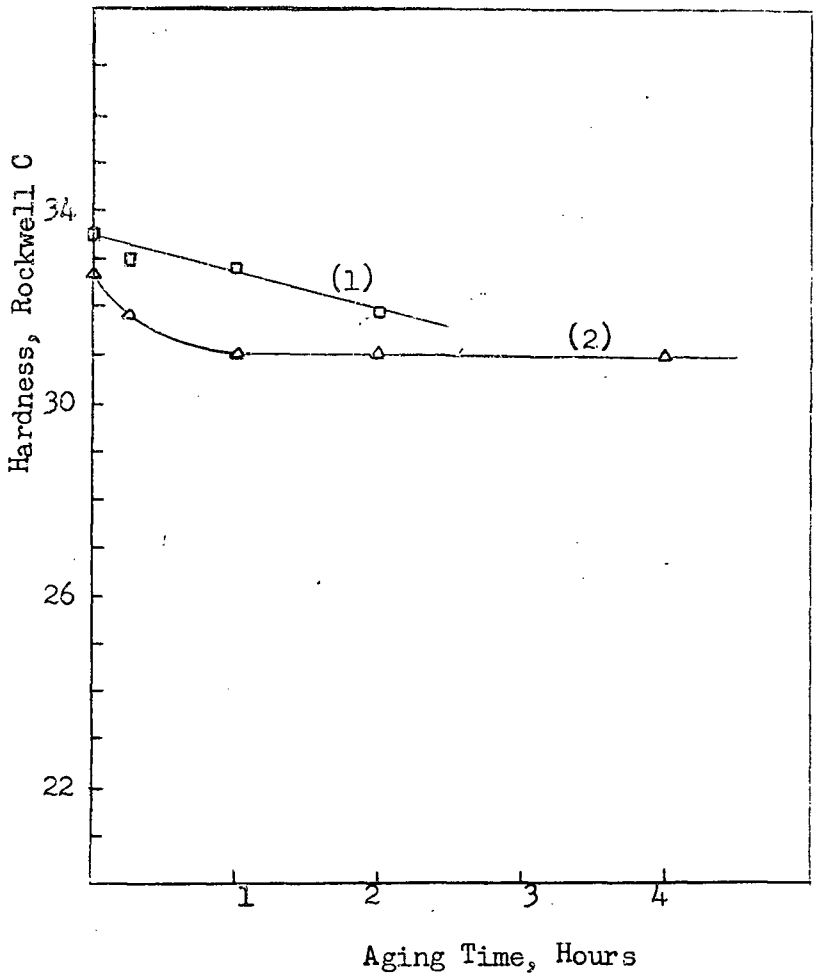

Fig. 38. Fe - 4.79% Si - 8.08% Mn. Aging Curves.
- Homogenized 1100° C, 24 Hours.
- Hotrolled 900° C.
- Annealed 900° C, 1 Hour.
  Curve (1) Air Cooled, Aged 600° C.
  Curve (2) Water Quenched, Aged 600° C.

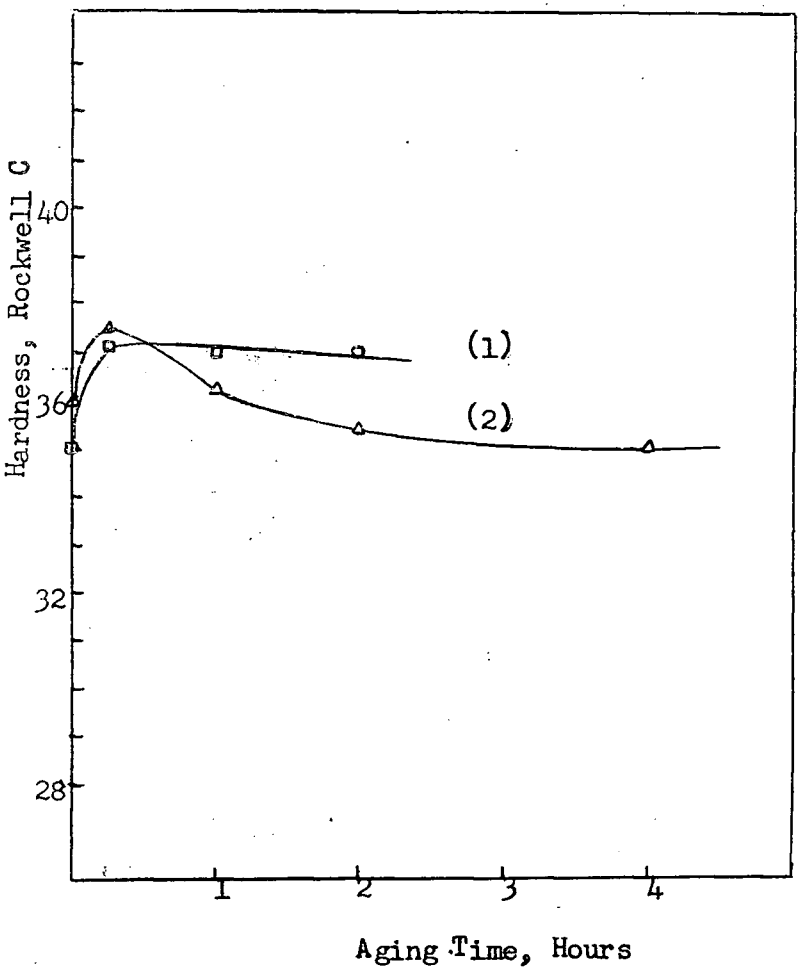

Fig. 39. Fe - 5.15 % Si - 9.43% Mn. Aging Curves.
- Homogenized 1100° C, 24 Hours.
- Hotrolled 900° C.
- Annealed 900° C, 1 Hour.
  Curve (1), Air Cooled, Aged 600° C.
  Curve (2), Water Quenched, Aged 600° C.

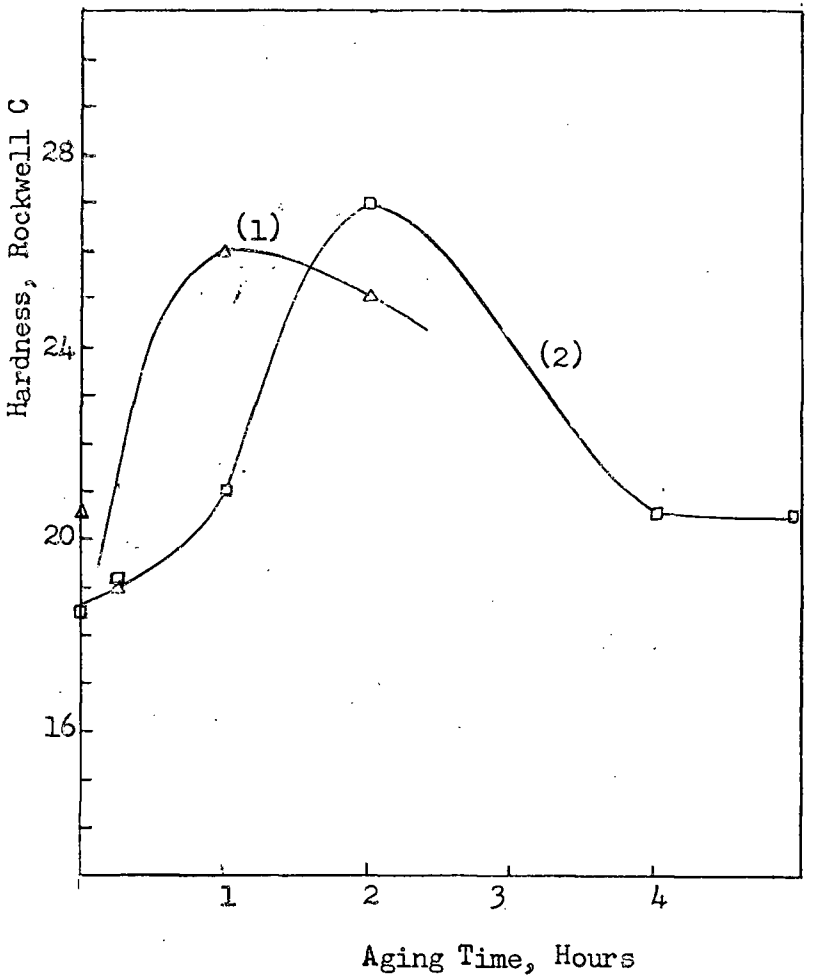

Fig. 40. Fe - 5.93% Si - 13.58% Mn. Aging Curves
- Homogenized 1100° C, 24 Hours.
- Hotrolled 900° C.
- Annealed 900° C, 1 Hour
  Curve (1) Air Cooled, Aged 600° C.
  Curve (2) Water Quenched, Aged 600° C.

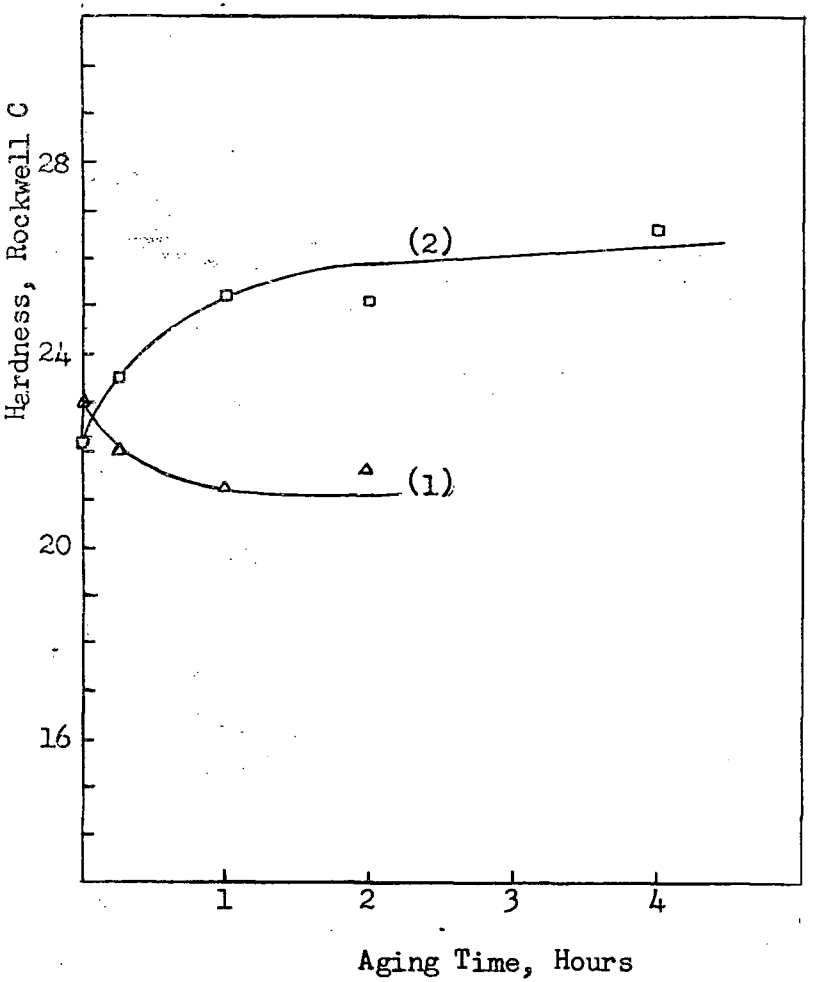

Fig. 41. Fe - 6.30% Si - 19.40% Mn. Aging Curves
- Homogenized 1100° C, 24 Hours.
- Hotrolled 900° C.
- Annealed 900° C, 1 Hour.
  Curve (1) Air Cooled. Aged 600° C.
  Curve (2) Water Quenched, Aged 600° C.

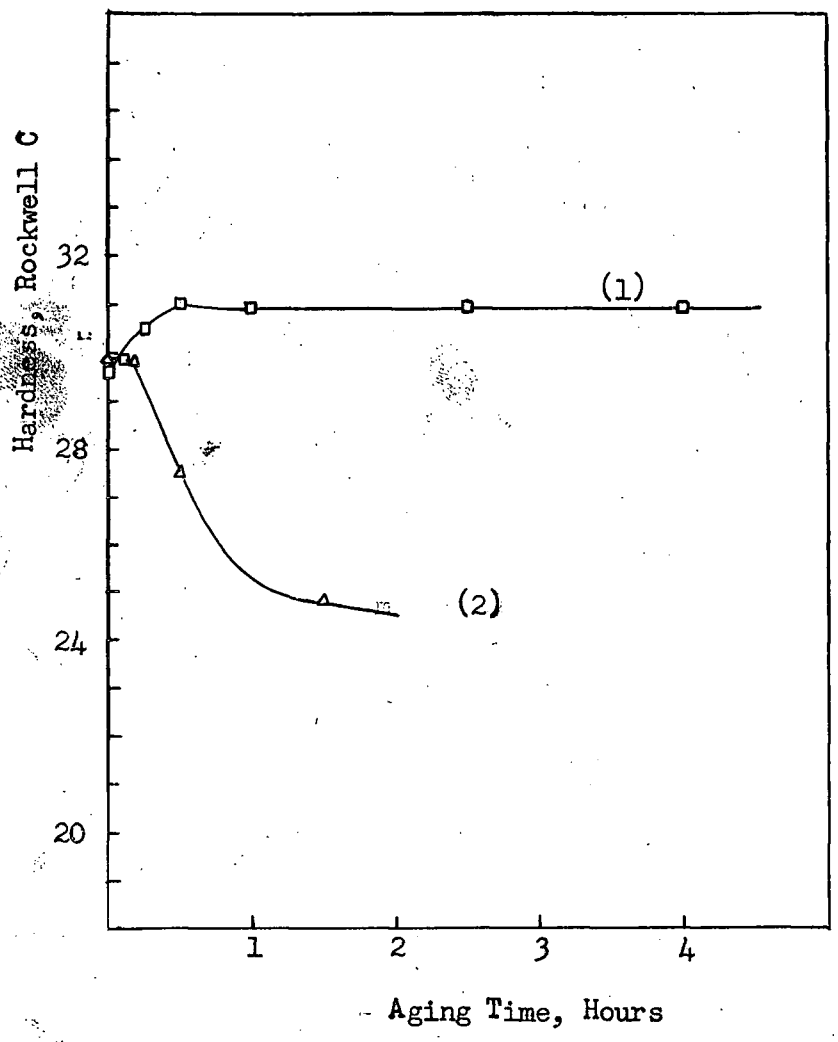

Fig. 42. Fe - 2.5% Si - 6.0% Mn - 0.5% Ti. Aging Curves
- Hotrolled 950° C.
- Annealed 950° C, 1/2 hour, Air Cooled.
- Curve (1) Aged 400° C.
  Curve (2) Aged 500° C.

REFERENCES

(1) M. J. Bibby and J. Gordon Parr: JISI, 202, 1964, 100 - 104.

(2) C. M. Wayman and C. J. Altstetter: Acta Met., 10, 1962, 992.

(3) C. M. Wayman: "Introduction to the Crystallography of Martensitic Transformations" MacMillan series in material science, 1964.

(4) A. B. Greninger and A. R. Troiano: Trans. AIME, 140, 1940, 307.

(5) J. S. Bowles: Acta Cryst., 4, 1951, 162 - 171.

(6) P. M. Kelly and J. Nutting: JISI, 197, 1961, 199.

(7) R. F. Mehl, C. Barrett and D. Smith: Trans. AIME, 105, 1933, 215.

(8) W. S. Owen, E. A. Wilson, T. Bell: "High Strength Materials"; Second International Materials Symposium, University of California. Wiley, New York, 1964.

(9) H. M. Otte and T. A. Read: Trans. AIME, 209, 1957, 412.

(10) J. F. Breedis and C. M.Wayman: Trans. AIME, 224, 1962, 1128.

(11) M. S. Wechsler, D. S. Lieberman and T. A. Read: Trans. AIME, 197, 1953, 1503.

(12) D. S. Lieberman, M. S. Wechsler and T. A. Read: J. Appl. Phys. 26, 1955, 473.

(13) J. S. Bowles and J. K. MacKenzie: Acta Met. 2, 1954, 129.

(14) R. Bullough and B. A. Bilby : Proc. Phys. Soc. Lond. B, LXIX, 1956, 1276.

(15) B. A. Bilby and J. W. Christian: "The Mechanism of Phase Transformations in Metals" Institute of Metals (London) monograph and report series No. 18.

(16) B. A. Bilby and J. W. Christian: JISI, 197, 1961, 122.

(17) J. W. Christian: "The Theory of Transformation in Metals and Alloys" Pergamon Press, 1965.

(18) D. S. Lieberman and R. Bullough: Phys. Status Solidi, 12, 1965, 675.

(19) M. S. Wechsler, T. A. Read and D. S. Lieberman: Trans. AIME, 218, 1960, 202.

(20) H. M. Otte: Trans. AIME, 218, 1960, 342.

(21) A. G. Crocker and B. A. Bilby: Acta Met., 9, 1961, 678.

(22) T. Honma: J. Japan Inst. Metals, 21, 1957, 51 - 55, 122 - 125, 126 - 128, 263 - 267.

(23) J. A. Klostermann and W. G. Burgers: Acta Met., 12, 1964, 355.

(24) H. Warlimont: Trans. AIME, 221, 1961, 1270.

(25) G. Thomas: "Transmission Electron Microscopy of Metals " John Wiley & Sons Inc., 1962.

(26) P. Dornen and W. Hofmann: Arch. Eisenh., 30, 1959, 627 - 636.

(27) H. Margenau and G. M. Murphy: "The Mathematics of Physics and Chemistry" D. Van Nostrand Co., Inc.

(28) H. Goldstein: "Classical Mechanics", Addison - Wesley Publishing Company Inc.

(29) M. S. Wechsler : Acta Met., 7, 1959, 793.

(30) D. Tromans: Dept. of Metallurgy, University of British Columbia; Private Communication.

(31) R. F. Decker, J. T. Eash, A. J. Goldman: ASM Trans. Quart. 55, 1962, 58.

(32) E. P. Sadowski: ASM Metals Eng. Quarterly, Feb. 1965, 56.

(33) J. R. Mihalisin: ASM Trans. Quart., 59, 1966, 60.

(34) G. P. Miller, W. I. Mitchell: JISI, 203, 1965, 895.

(35) S. Floreen, G.R. Speich: ASM Trans. Quart., 57, 1965, 645.

(36) Seminar on Maraging Steels, International Nickel Co., April, 1962.

(37) W. R. Patterson, L. S. Richardson: ASM Trans. Quart, 59, 1966, 71.

(38) A. J. Goldman, J. Manenc : ASM Trans. Quart., 58, 1965, 645.

(39) Keiichi Ohta: Technol. Repts., Kansai Univ. 1, No. 1, 65 - 71 (1959).

(40) J. R. Kattus: Southern Research Institute, Birmingham, Albama, Private Communication, Sept. 1966.

(41) L. S. Richardson: Foote Mineral Company, Exton, Penna, Private Communication April, 1966.

(42) A. R. Troiano, F. T. McGuire: ASM Trans. Quart., 31, 143, 340.

(43) H. M. Otte: Acta Met., 5, 1957, 614.

(44) D. W. Gomersall, J. G. Parr: JISI, 203, 1965, 275.

(45) R. P. Reed: Acta Met., 10, 1962, 865.

(46) J. F. Breedis and W. D. Robertson: Acta Met., 10, 1962, 1077.